INFORMATION TO USERS

This material was produced from a microfilm copy of the original document. While the most advanced technological means to photograph and reproduce this document have been used, the quality is heavily dependent upon the quality of the original submitted.

The following explanation of techniques is provided to help you understand markings or patterns which may appear on this reproduction.

1. The sign or "target" for pages apparently lacking from the document photographed is "Missing Page(s)". If it was possible to obtain the missing page(s) or section, they are spliced into the film along with adjacent pages. This may have necessitated cutting thru an image and duplicating adjacent pages to insure you complete continuity.

2. When an image on the film is obliterated with a large round black mark, it is an indication that the photographer suspected that the copy may have moved during exposure and thus cause a blurred image. You will find a good image of the page in the adjacent frame.

3. When a map, drawing or chart, etc., was part of the material being photographed the photographer followed a definite method in "sectioning" the material. It is customary to begin photoing at the upper left hand corner of a large sheet and to continue photoing from left to right in equal sections with a small overlap. If necessary, sectioning is continued again — beginning below the first row and continuing on until complete.

4. The majority of users indicate that the textual content is of greatest value, however, a somewhat higher quality reproduction could be made from "photographs" if essential to the understanding of the dissertation. Silver prints of "photographs" may be ordered at additional charge by writing the Order Department, giving the catalog number, title, author and specific pages you wish reproduced.

5. PLEASE NOTE: Some pages may have indistinct print. Filmed as received.

University Microfilms International
300 North Zeeb Road
Ann Arbor, Michigan 48106 USA
St. John's Road, Tyler's Green
High Wycombe, Bucks, England HP10 8HR

77-32,050

KRASNEY, Stuart, 1941-
MOSSBAUER SPECTROSCOPIC INVESTIGATIONS OF HEMOGLOBIN AND μ-OXO-BIS PORPHYRIN COMPLEXES.

City University of New York,
Ph.D., 1977
Biophysics, general

University Microfilms International, Ann Arbor, Michigan 48106

MOSSBAUER SPECTROSCOPIC INVESTIGATIONS OF HEMOGLOBIN AND μ-OXO-BIS PORPHYRIN COMPLEXES

by

STUART KRASNEY

A dissertation submitted to the Graduate Faculty in Physics in partial fulfillment of the requirements for the degree of Doctor of Philosophy, The City University of New York.

1977

This manuscript has been read and accepted for the Graduate Faculty in Physics in satisfaction of the dissertation requirement for the degree of Doctor of Philosophy.

September 12, 1977
date

Melvin Lax
Professor Melvin Lax
Chairman of Examining Committee

September 12, 1977
date

Miriam P. Sarachik
Professor Miriam Sarachik
Executive Officer

Dr. Thomas H. Moss
Dr. Gerald A. Corker
Professor Robert R. Alfano
Professor Ying Wei Chow

Supervisory Committee

The City University of New York

Abstract

MOSSBAUER SPECTROSCOPIC INVESTIGATIONS OF HEMOGLOBIN AND μ-OXO-BIS PORPHYRIN COMPLEXES

by

Stuart Krasney

Adviser: Professor Melvin Lax

We have built a computer controlled high precision Mossbauer spectroscopy apparatus and used it to investigate the hyperfine interactions of Fe^{57} and its surrounding heme in oxyhemoglobins and antiferromagnetically coupled μ-oxo-bis porphyrin complexes. We have found a distinct difference in the Mossbauer quadrapole splitting energy separations of Rhesus monkey oxyhemoglobin in the cellular environment as compared to that in solution. We attribute this difference in part to the binding of 2,3-Diphosphoglycerate by the hemoglobin in the cell. We have found no measurable differences in the Mossbauer spectra of the oxyhemoglobins over a pH range of 6.9 to 7.7. Our Mossbauer data for the μ-oxo-bis porphyrin complexes reveal a temperature dependent asymmetry which we attribute to a vibrational anisotropy of the iron atoms in the lattice. Our data for these μ-oxo-bis complexes compare favorably with a theoretical model based on contributions from both the optical and acoustical vibrational modes. We confirm that the iron-oxygen-iron bond angles of the μ-oxo-bis complexes govern the crystal field contribution to the electric field gradient at the iron nucleus. We also correlate electric field gradient nuclear interactions with molecular symmetries of these complexes and with steric hindrances induced by bulky side chains on the porphyrin ring.

ACKNOWLEDGMENTS

I wish to thank Dr. Thomas H. Moss, formerly of the IBM Thomas J. Watson Research Center, and Professor Melvin Lax of the City College of New York for their continuing counsel during this work. I would also like to thank Dr. Philip Aisen of the Albert Einstein Medical Center and his staff for their assistance in the Fe^{57} enrichment of rabbit hemoglobin and Dr. Wendall Nieman of the New York University Laboratory for Experimental Medicine on Primates and his staff for their assistance in the Fe^{57} enrichment of Rhesus monkey hemoglobin. Additionally, I would like to thank Professor Winslow Caughey of Colorado State University for the preparation of the μ-oxo-bis porphyrin complex samples.

Finally, my thanks to Mrs. Dorothy Brinkley and Mrs. Ann Carol Hohl for their assistance in typing and proofreading this manuscript.

Dedicated to Isabelle and Sara.

TABLE OF CONTENTS

LIST OF TABLES

LIST OF FIGURES

INTRODUCTION

Iron complexes are found in many important proteins such as hemoglobin, myoglobin, transferrin and various cytochromes and are critical to the diverse function of these molecules. Many proteins with iron porphyrin complexes exhibit very different functions. This suggests that subtle differences in the local environment of the iron ions are important in determining the function of these proteins. Mossbauer spectroscopy is one of the most sensitive methods for investigating the electronic state of the iron ions through the interaction of the electrons with the iron nucleus via the electric field gradient and magnetic splittings of the atomic nuclear quantum states. By measurement of such interactions, data acquired from Mossbauer spectroscopy has contributed information useful in the understanding of the structure-function relationship of some of these proteins.

Until recently, Mossbauer spectroscopy of iron proteins has focused upon the measurements of isomer shifts and the quadrapole splittings of different complexes. Correlations between the experimentally measured values for these parameters and the physical conditions existing within the molecules have been very difficult in view of the vastly complex structure of many of the proteins investigated. With the additional contributions to the hyperfine Mossbauer spectra of magnetic effects (due to paramagnetism in the sample and/or the presence of laboratory generated fields), the comparison of theoretical models began to yield more insight into the nature of the environment of the iron atom.

A class of iron proteins in which the iron atom(s) are known to be at the center of a prosthetic group known as the porphyrin has been the subject of many Mossbauer studies. A member of this class of heme-proteins which is extremely important to humans is hemoglobin. Scientific studies of this molecule have been carried out using many available methods including Raman spectroscopy, laser flash photolysis, nuclear and electron paramagnetic resonance and Mossbauer spectroscopy. By building a Mossbauer apparatus capable of highly accurate measurements we have studied differences in hyperfine parameters which up until

now have been in the region of statistical error. We have determined that the sites of the iron atoms in hemoglobin are affected by removing the hemoglobin molecule from its natural environment (the red blood cell). In view of the comparisons between hemoglobin samples where the small naturally occurring molecule 2,3-Diphosphoglycerate (DPG) had been 'stripped', and samples where it had not been 'stripped', experimental evidence suggests that DPG bound to hemoglobin in the cell may be the cause for the observed differences. This result may be of extreme importance in view of the regulatory function of DPG on the oxygen affinity of this molecule. We have also found that there is no measurable difference between hemoglobins when the amino acid compositions are different (comparative studies between rabbits and monkeys), and that pH dependent effects on the hemoglobin in solution could not be detected within experimental accuracy of our apparatus.

Another group of heme-iron complexes are those in which two porphyrin rings form dimers when the atoms are anti-ferromagnetically coupled by a single oxygen atom. Much interest has been stimulated in these μ-oxo-bis coupled complexes since it is believed they are characteristic of the iron sites in some other important proteins. By careful analysis of spectra of six of these complexes, we hope to add to the understanding of their structure. Perhaps the most significant physical finding in our work is the observation of the temperature dependent vibrational anisotropy (the Gold'anskii Karyagin effect) in these μ-oxo-bis iron complexes. This effect has, up until now, been verified in only Tin and Iodine compounds, and thus we report the first detailed experimental observation of this effect in iron complexes. Our data are in good agreement with a theoretical model based on both discrete and continuous vibrational mode contributions.

THEORY OF THE MOSSBAUER EFFECT

In a solid, the fraction of γ-rays emitted or absorbed without energy loss is given by[186]

$$f = \exp(-\langle L_i \mid X_k^2 \mid L_i \rangle / \lambda^2) \quad (1)$$

where X_k is the component of the vector in the direction of the emitted photon and $|L_i\rangle$ represents the state of the lattice before (and after the emission (absorption)) of the photon, (Fig. 1). The classical analogue of (1) is given by[63]

$$f = \exp(-\langle X^2 \rangle / \lambda^2) \quad (2)$$

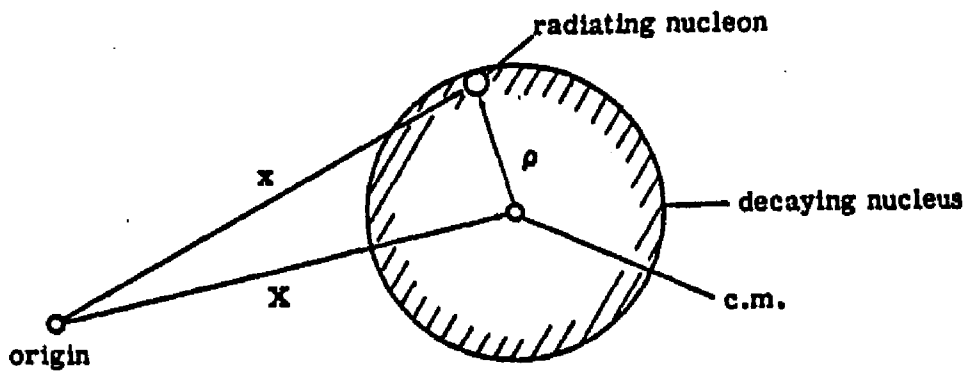

Figure 1 Coordinates for evaluation of equation (1).

For a solid, there are two simple models for the vibrational spectra; one corresponding to a continuum of acoustical modes (the Debye Model) and the other corresponding to discrete optical modes (the Einstein Model).

The corresponding expressions for the Mossbauer fractions are then [191]

$$F_{acc} = (9\hbar^2)/(4mk_b\Theta_d)\ \{1 + (4T^2)/(\Theta_d^2)\ \int_0^{\Theta_d/T} udu/(e^u-1)\}\ \text{(Debye Model)} \quad (3)$$

$$F_{opt} = \exp\ [-(E_r)/(\hbar\omega_0)\ \coth\ (\hbar\omega_0/2k_bT)]\ \text{(Einstein Model)} \quad (4)$$

In many solids it is possible to assume the Mossbauer spectrum as arising from a Debye model. In biological solids however, the nature of the solid is much more complicated. For example, hemoglobin, a molecule of approximately 67,000 gmw with four iron atoms can certainly not be considered as having a single iron atom per unit cell. Indeed, a more accurate

representation of the solid must include contributions to the recoilless fraction from both continuous and discrete vibrational modes. This fact will be considered in detail in the section on the asymmetric properties of the Mossbauer spectra.

An atom with a nuclear spin greater than 1/2 possesses a nuclear quadrapole moment.[127] The interaction energy of a non-zero electric field gradient and a nuclear quadrapole moment Q is given by[78,107]

$$E_q = (e^2qQ)/(4I(2I-1))\,[3I^2_z - I(I+1)]\,(1 + (\eta^2)/(3))^{1/2} \qquad (5)$$

where q is the component of the second derivative of the electrostatic potential in a coordinate system aligned to make the off diagonal elements of the field gradient tensor equal to zero, $\eta = (q_x - q_y)/q_z$ and $q_z = q_0$.

In the absence of magnetic effects, Fe^{57} with $I_g = 1/2$, $I_{ex} = 3/2$, the electric field gradient-nuclear quadrapole interaction (excited state only) will produce transitions as shown in Fig. 2.

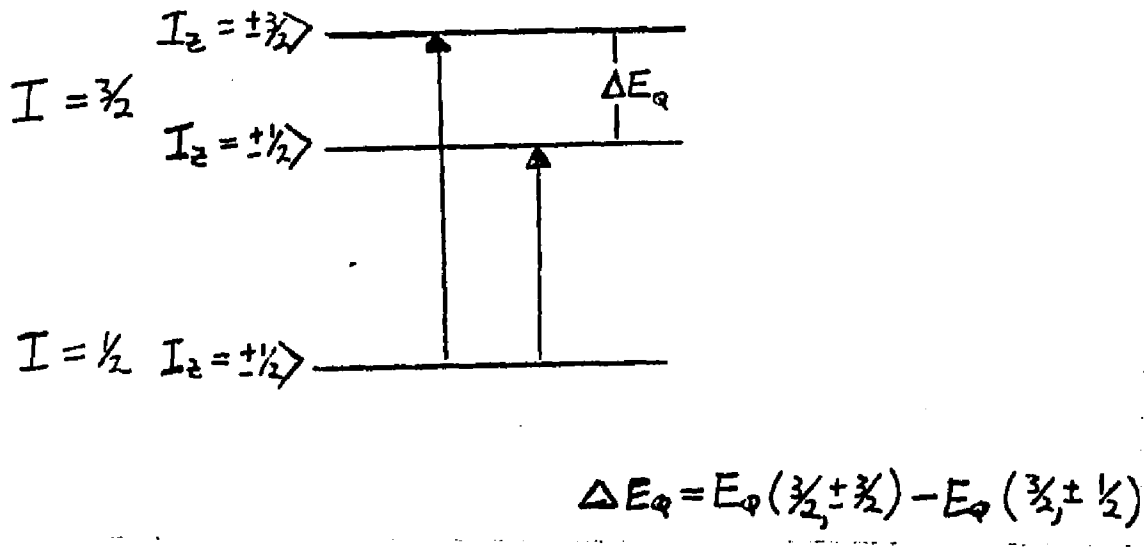

Figure 2 Electric field gradient nuclear quadrapole transitions of Fe^{57}.

For a simple EFG nuclear quadrapole moment interaction in the absorber, the Mossbauer spectrum obtained is typical of Fig. 3.

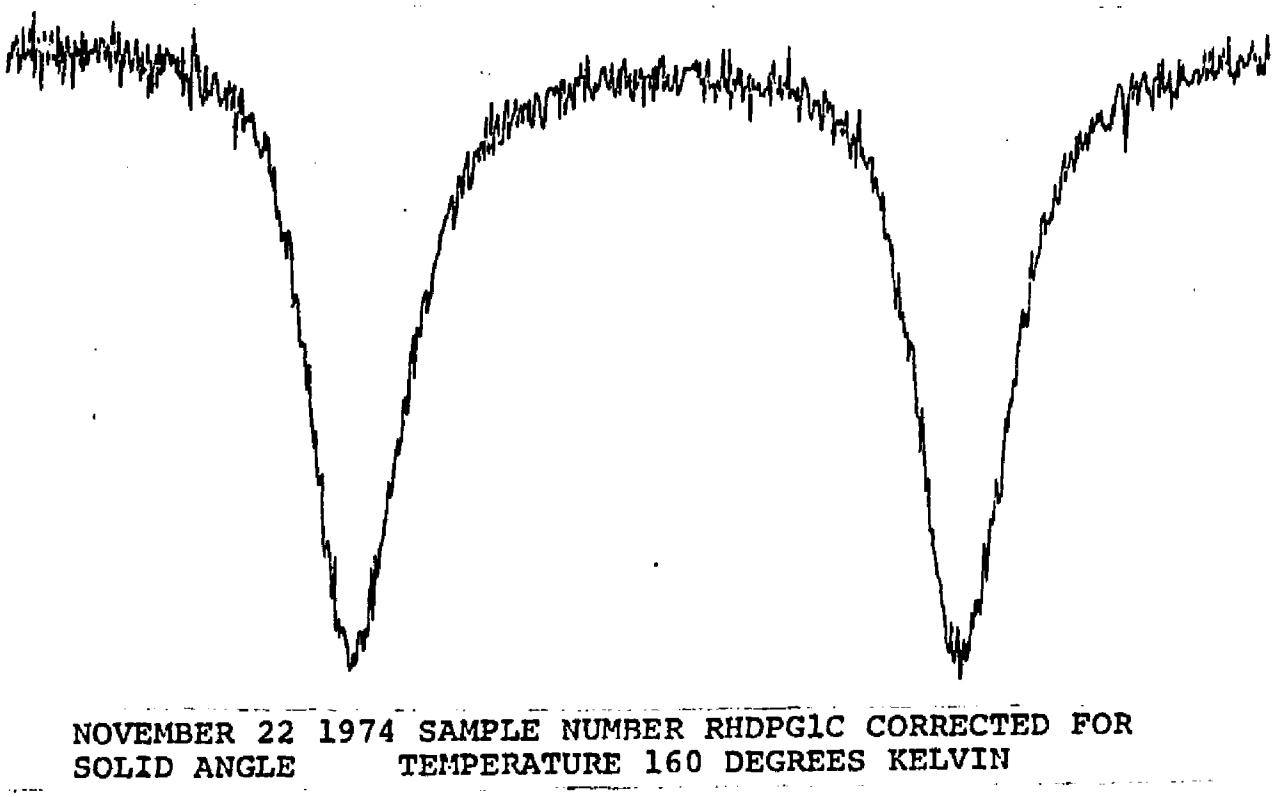

Figure 3 Relative transmission vs. velocity (−3 to +3 mm/sec).

The isomer shift due to differences of the physical surroundings of the nuclei of the absorber and the source is given by[191]

$$\text{I.S.} = (4\pi/5)\, Ze^2R^2\, (\delta R/R)\, (\, |\, \psi(o)\, |^2_{abs} - |\, \psi(o)\, |^2_{source}\,) \qquad (6)$$

where

$$R^2_{ex} - R^2_{gd} = R^2(\delta R)/(R). \qquad (6a)$$

Experimentally, this effect shifts the entire spectrum (similar to that shown in Fig. 3) to higher or lower energies. Magnetic hyperfine interactions are extremely complicated because they may produce interaction energies comparable to those due to EFG-quadrapole moment interactions.

The simple magnetic interaction term is

$$H_{mag} = -\mu \cdot H = -g\mu_n I \cdot H \tag{7}$$

with levels $E_m = -g\mu_n Hm_I$, $M_I = I, I-1,\ldots,-I$[191] where μ_n is the nuclear magneton and g is the nuclear g-factor (Figs. 4 and 5).

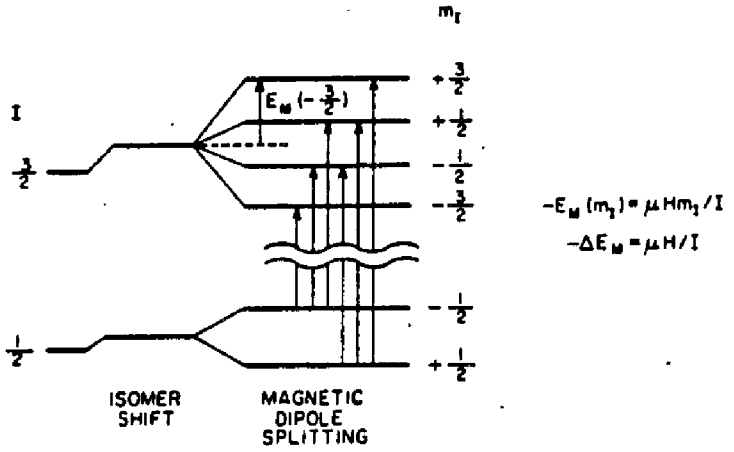

Figure 4 Energy levels of the magnetic interaction.

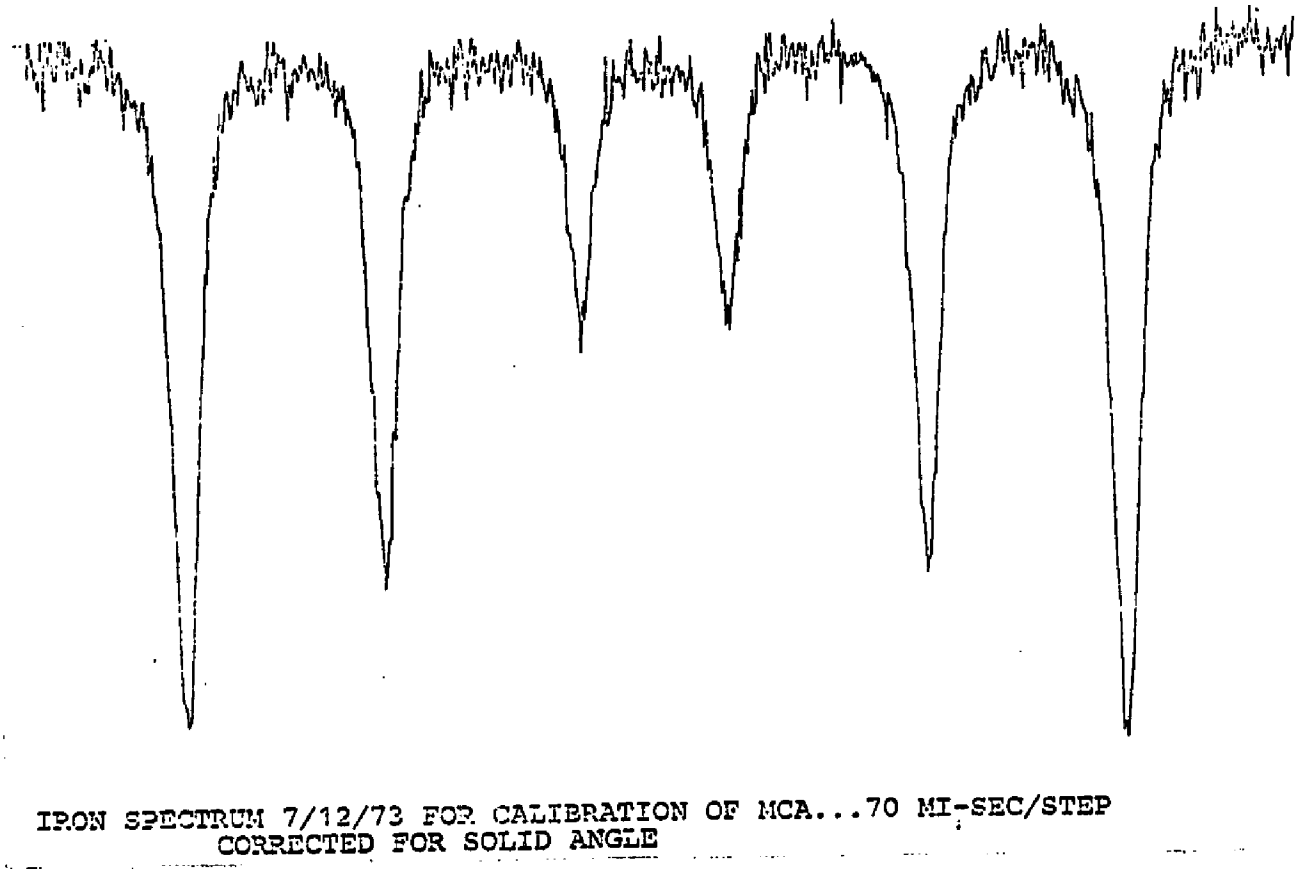

Figure 5 Relative transmission vs. velocity (−10 to +10 mm/sec).

The intensities of the separate lines are calculated by the evaluation of the Clebsch-Gordan coupling coefficients[49]

$$| I_e m_e> = \Sigma <I_g J_{ms} (m_e - m_g) | I_e m_e> | JM> | I_g m_g> \quad (8)$$

and are shown in Fig. 6.

Transitions	Δm	Total	Angular dependence
$\frac{3}{2} \rightarrow \frac{1}{2}$ $-\frac{3}{2} \rightarrow -\frac{1}{2}$	-1 $+1$	3	$\frac{3}{4}(1 + \cos^2\theta)$
$\frac{1}{2} \rightarrow \frac{1}{2}$ $-\frac{1}{2} \rightarrow -\frac{1}{2}$	0 0	2	$3 \sin^2\theta$
$-\frac{1}{2} \rightarrow \frac{1}{2}$ $\frac{1}{2} \rightarrow -\frac{1}{2}$	$+1$ -1	1	$\frac{3}{4}(1 + \cos^2\theta)$

Figure 6 Clebsch-Gordan coefficients of the magnetic interaction transition probabilities.

When θ is averaged over all angles (to account for all directions of magnetic domains in iron) the ratio of the outer to middle to inner lines is 4:3:2.[4]

EXPERIMENTAL APPARATUS

A Northern Scientific Model NS-700 Pulse Height/Multichannel Analyzer was used for all data acquisition. A Reuter-Stokes RSG-61 proportional counter (Krypton, Methane) was used as a detector to input to an Ortec 109PC pre-amplifier. The pulse height spectrum thus obtained from our source, Co^{57} in a Rhodium Matrix, and its decay scheme are shown in Figs. 7 and 8.

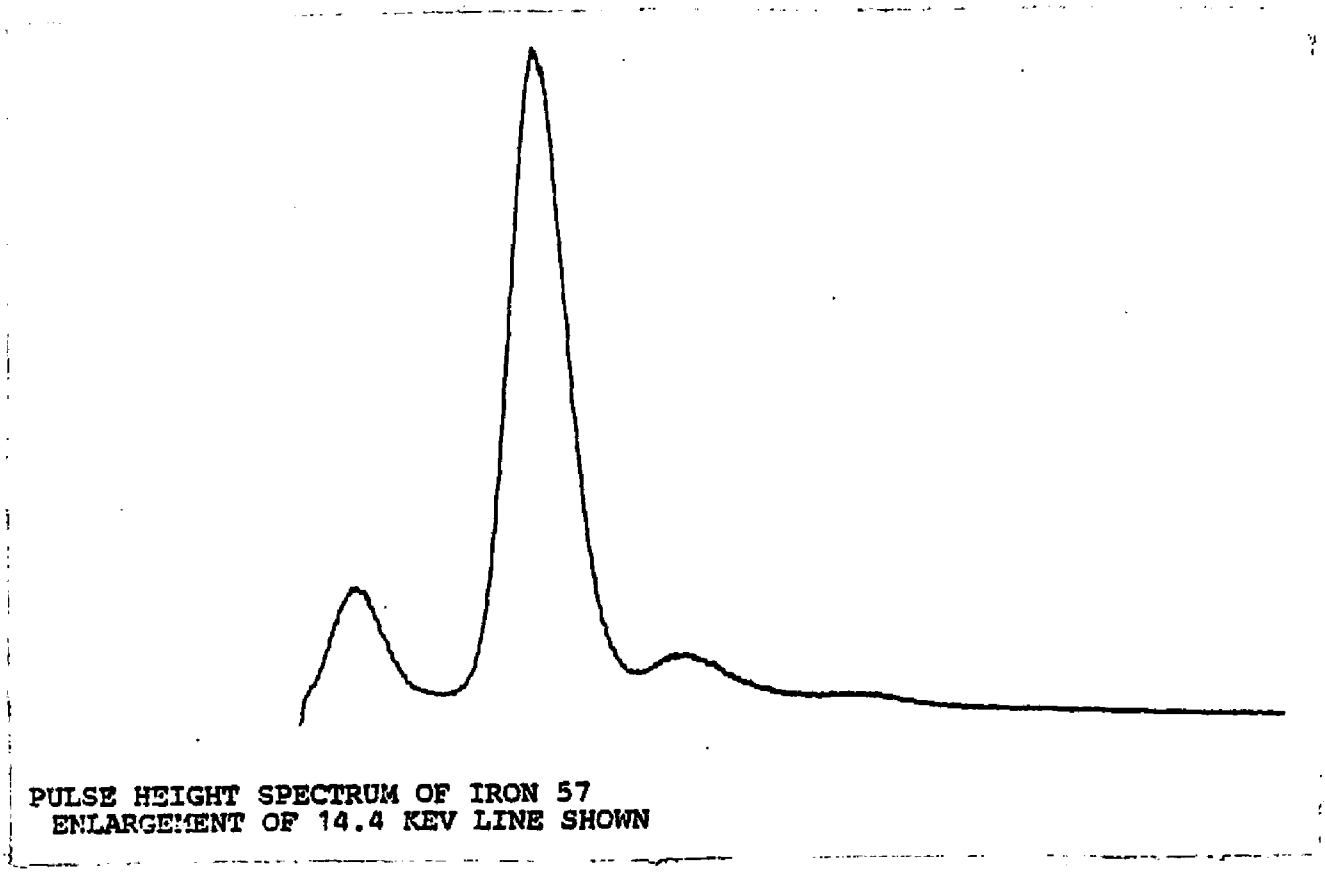

Figure 7 Number of counts vs. energy.

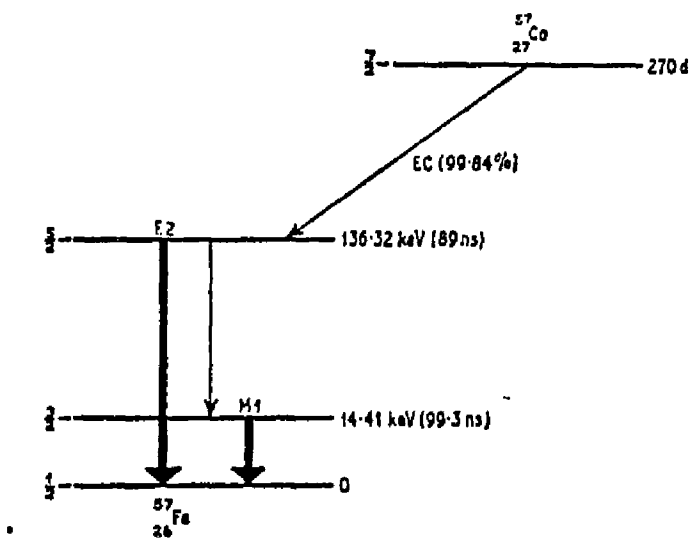

Figure 8 Co^{57} nuclear decay scheme.

In the multichannel analyzer mode, the NS-700 was driven by an Elscint Mossbauer Function Generator Model MFG-2. The source was mounted at the end of a moving shaft of an Elscint MVT-2 Linear Velocity Transducer coupled to the MD-2E transducer drive unit. In the mode most commonly used, the physical motion of the transducer was parabolic producing a constant acceleration of the moving shaft giving a velocity linear in time.

The cryostat was manufactured to specification by the Magnetic Corporation of America. It consisted of a liquid nitrogen container separated from the outside jacket and liquid helium region by a 'vacuum' space. A 'well' at the bottom of the dewar was the housing for a superconducting magnet wherein the sample holder was suspended on a hollow stainless steel shaft (Fig. 9). The sample holder was machined from solid copper and a 1 cm diameter hole was drilled through. The samples were placed in polyethylene vials of 1 cm outer diameter and approximately .5 cm in length. These fit snugly into the copper sample holder to insure good thermal contact. A teflon spacer slightly larger than the sample holder kept the sample holder in place with respect to the cavity of the magnet. Four holes were drilled through the sample holder near the central hole and four 1/8 watt 100 ohm resistors wired in parallel could then heat the sample uniformly. An additional 100 ohm resistor was inserted

into another hole near the center to monitor the temperature when liquid helium was used. A copper constantin thermocouple was attached at the top of the sample holder to monitor temperatures between 77° and 300° Kelvin. (Fig. 9a).

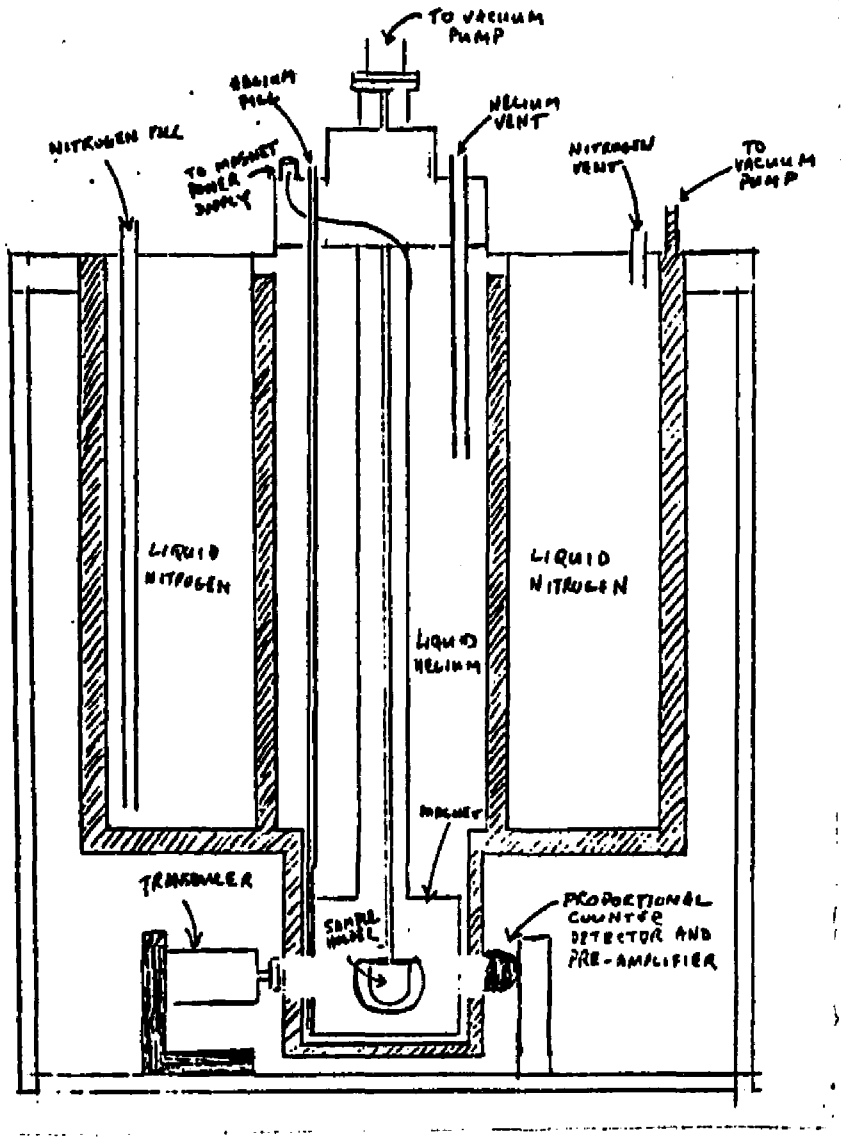

Figure 9 Cryostat for Mossbauer samples; source and detector positioning.

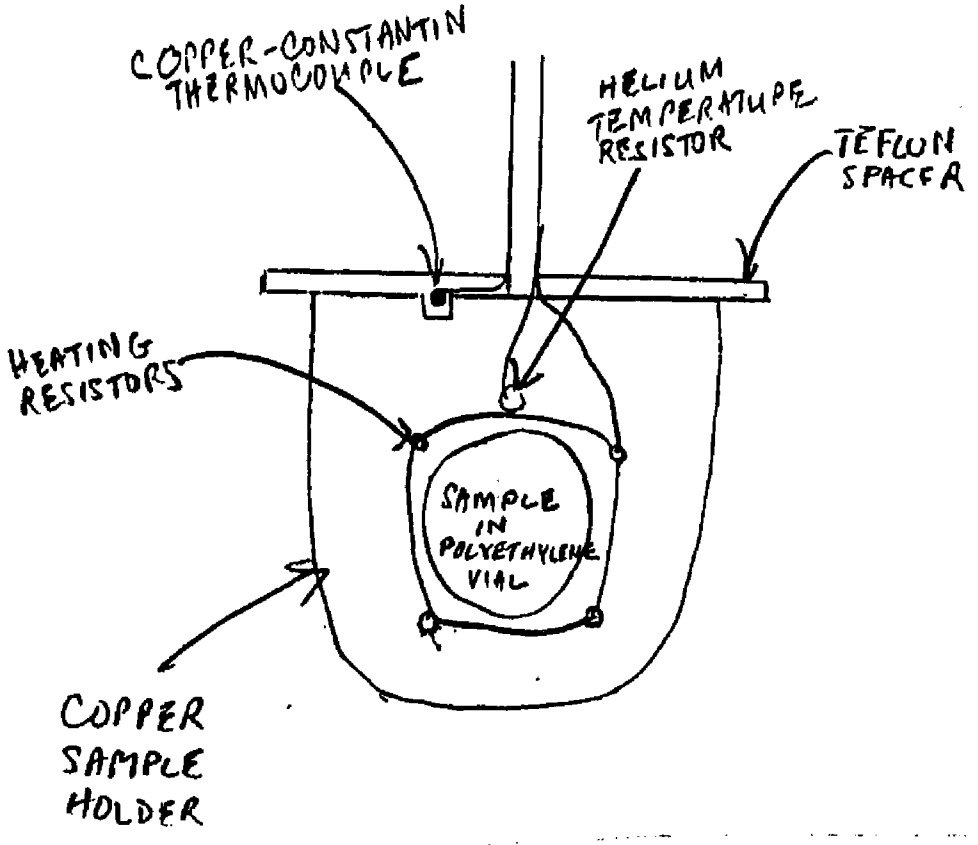

Figure 9a Sample holder.

All the 'windows' in the dewar and sides of the magnet were made of 4 mil mylar and held in place with Torr Seal low vapor pressure epoxy resin. The super conducting magnet could attain fields of up to 35 kilo-gauss. The entire dewar could be rotated by 90° enabling the axis of the magnet to be aligned either perpendicular or parallel to the direction of the incident γ-photon beam.

COMPUTERIZATION OF THE EXPERIMENT

Each spectrum was collected and stored in 1023 discrete channels of the Multi Channel Analyzer. With as many as four spectra being accumulated in a 24 hour period, the need for an efficient and rapid method of saving the information was obvious. Furthermore, if one is to have rapid access to past records (as well as current) in order to do numerical analysis, an efficient method of file management is also needed.

The host system chosen was an IBM System 370, Model 145 running CMS under VM. CMS is an interactive time shared system where each user is in control of his own virtual computer. Access to the system was via a telephone dataset using a remote communications terminal (IBM #2741). The Research Device Coupler[105,106] (RDC) is an internally developed interface designed to communicate with a host computer in much the same way as a communications terminal. In the case of this experiment, the RDC was directly wired to a port on an IBM 2701 communication adapter installed on the 370/145. The transmission link on this line was 600 baud (versus 134 baud) over the data set link. The data transmission rate was approximately 65 characters/sec. Each channel of the MCA contained six BCD digits, thus its memory could be 'dumped' to the host in about 1 1/2 minutes.

The RDC is a set of individual modules in a self-contained interface which through its System Coupler Module (SCM) is capable of addressing the other modules and transmitting any data from these to the host system. Additionally, a 10 bit D/A converter in the RDC was used to drive a Tektronix Storage Display Scope for the graphical display of data. A complete RDC is shown in Fig. 10.

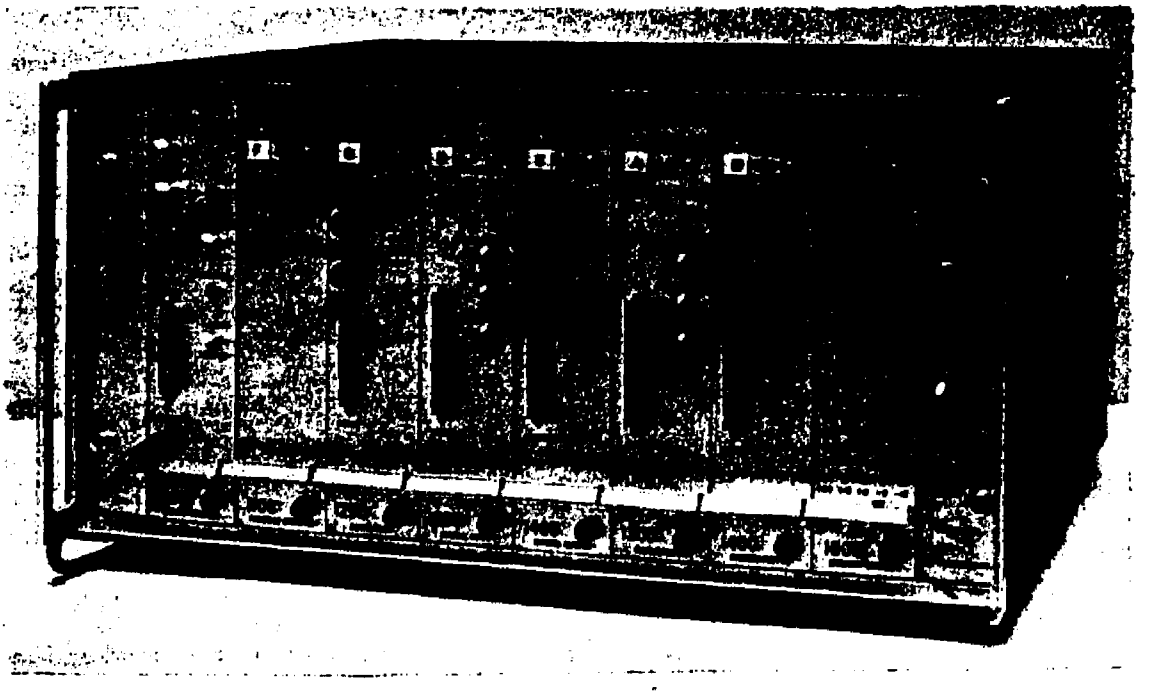

Figure 10 Research Device Coupler.

All of the Device Coupler programming for this experiment was done in FORTRAN IV using general purpose RDC auxiliary processor assembler language routines for I/O.

The need for simplicity of operation of programming is important if efficiency is desired. Interactive programming is not a new concept and although certain computer languages are interactive by design (e.g., APL), a particularly new approach was taken in the case of FORTRAN IV, by the inclusion of FISLIB. All programming for control of the experimental hardware, data reduction and graphics was made a totally interactive conversational package of simple user commands at a terminal.

The FORTRAN Interactive Subroutine Library (FISLIB) was developed at the Thomas J. Watson Research Center for inclusion in any user written FORTRAN program. Although FISLIB was developed as a general purpose set of routines, many specifications as well as actual code resulted from our work.

Proper use of this package allows a user to interact with his program in a totally free-form style. It essentially allows one to convert a FORTRAN program into one in which

the user defines his own unique command language. Thus, for example, the command DUMP entered at the terminal would result in our program's addressing the RDC and instructing it to dump the MCA data to the host system. The two most important considerations here are:

a) although the actual programming necessary to interpret these commands is detailed, the application program is simple to use.

b) because the host system on which the program is running is an interactive one, the completion of execution of each command is followed by a request for the next.

The size of the program is relatively unimportant since the VM/370 will dynamically segment the executable code and allow only as much main storage as is necessary for the completion of each segment. When the 'dump' was complete, the information in main storage was written to a disk for permanent storage. In conjunction with each 'Raw Data' file was a file used to store data which had been processed. In this way, the Raw Data for each run was always saved. A complete discussion of the program command structure and function appears in Appendix I.

PRECISION OF EXPERIMENTAL DATA

All of the iron porphyrin data to be presented were collected with the MCA running in the constant acceleration mode using a velocity range of −.3 cm/sec to +.3 cm/sec. The dwell time in each channel was 70 μsec. As a check on reproducibility and accuracy of results, calibration spectra of iron foil were run periodically.

Over the period of approximately nine months' time when most of the spectra were collected, five calibration runs using iron foil were done at a temperature of 293° Kelvin. The parameters for channel/velocity conversion were determined from the first of these spectra using 1.677 mm/sec as the original input for the separation of the inner two lines.[160] The five measured separations based on a least squares Lorentzian fit of the inner two peaks yielded computed separations of 1.677, 1.679, 1.675, 1.677 and 1.677 mm/sec. These observed data result in a standard deviation of ±.0014 mm/sec.

One sample for which seven different spectra were acquired (under similar conditions) over a period of three months (an iron-porphyrin complex to be discussed later) at constant temperatures ranging between 144° and 160° Kelvin yielded quadrapole splittings of .55, .548, .550, .544, .545, .547 and .546 mm/sec respectively. The isomer shifts (relative to iron) were .375, .370, .374, .370, .367, .368 and .371 mm/sec. These observed data yield standard deviations of ±.0023 mm/sec and ±.0029 mm/sec. Figure 11 shows one of these spectra.

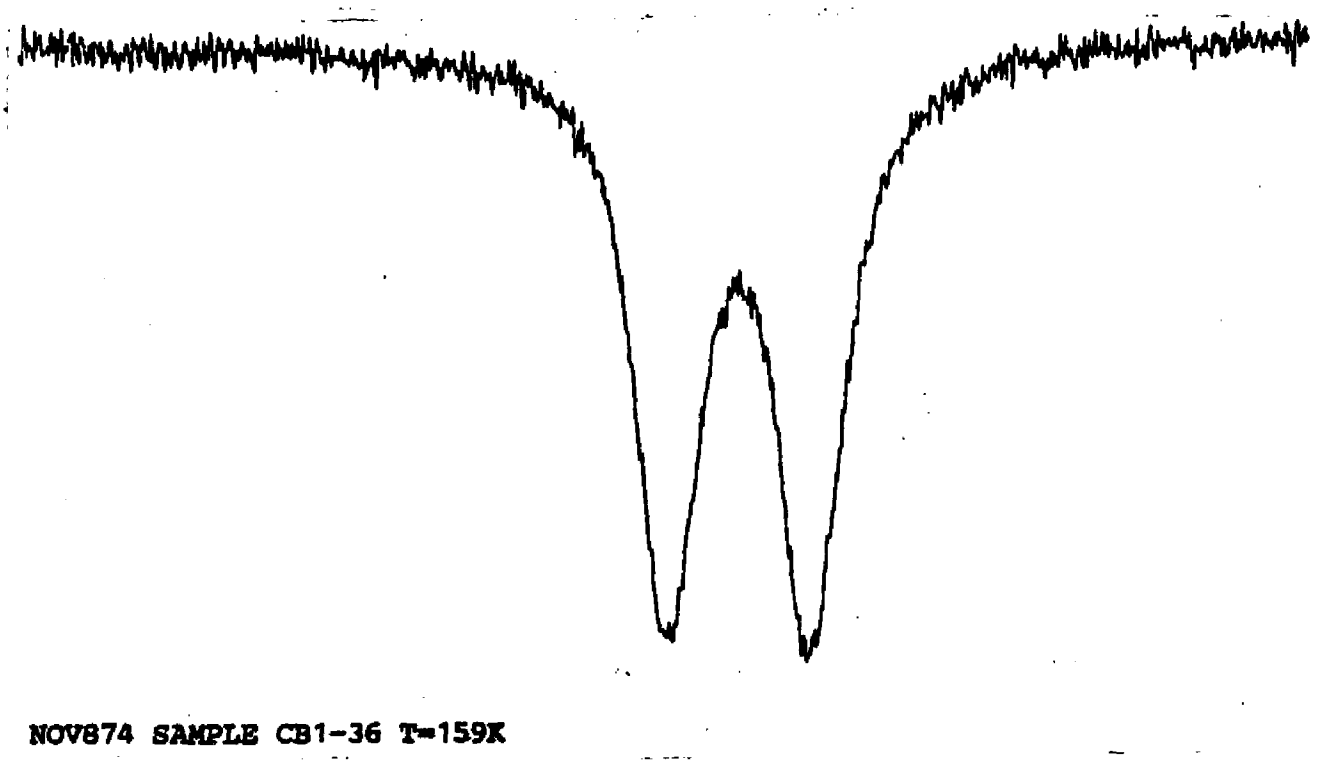

Figure 11 Relative transmission vs. velocity (−3 to +3 mm/sec).

In view of some generally quoted statistical accuracies of standard deviations in iron porphyrin complexes of ±.05 mm/sec[91] and ±.02 to ±.04 mm/sec[111] for example, the accuracy of our experimental results achieved is important.

HEMOGLOBIN AND IRON PORPHYRIN COMPLEXES

The porphyrin rings are derivatives of the parent porphin which consists of four pyrrole molecules bound into a cyclic structure by four methane bridges. The most commonly found porphyrin in nature is the one in which the pyrrole rings carry four methyl (CH_3), two vinyl ($CH{=}CH_2$) and two propionic acid (CH_2-CH_2-COOH) pyrrole substituents.[59] This complex is commonly referred to as protoporphyrin (IX) and is shown (along with the parent complex, porphin) in Fig. 12.

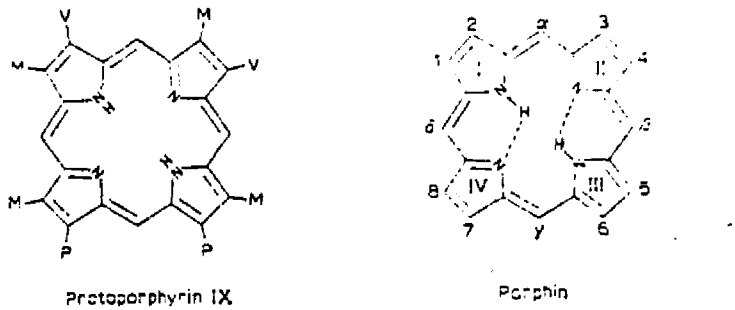

Figure 12 Structure of Protoporphyrin and Porphin.

The porphyrin ring just described with iron (II) at the center of the four nitrogen atoms and lying approximately in their plane is the prosthetic group that is responsible for the reversible binding of oxygen in such molecules as hemoglobin and myoglobin.[10] Other iron containing 'heme' porphyrin complexes investigated in our work are those in which the numbered 2 and 4 positions of the pyrrole rings have different groups substituted for the ethyl's. Before discussing some of these porphyrin complexes as individual entities, a brief discussion of the role of protoporphyrin IX iron (II) as the reversible binder of 0_2 (specifically in Hemoglobin) is in order. A complete review of the overall structure and function of hemoglobin is available in the works of Antonini and Brunori,[10] the monograph by Huisman and Schroeder,[90] and the book by Dickerson and Geis.[56]

From a biological viewpoint, hemoglobin will bind O_2 (become oxygenated) or it will release O_2 (become deoxygenated) at high and low partial pressures of oxygen respectively.

Physiologically, these events occur in the lungs and tissues respectively. Each of the four heme iron atoms per hemoglobin molecule is capable of binding a single O_2 molecule.

The 10,000 atoms of the hemoglobin protein consist of two identical sets of helical polypeptide chains (named 'α' and 'β') consisting of 141 and 146 amino acids respectively. Each of these 'α' and 'β' chains contains a hydrophobic pocket (formed by the bending of the helical super structure) wherein the heme complex is situated.

Oxygen binds to the sixth coordinate position of the iron atom forming an octahedral complex. The fifth position is occupied by the nitrogen atom of the proximal histidine amino acid side chain.[154] Figure 13 shows the amino acid structure of the α-helix chain. A typical plot of the fraction of oxygen bound to hemoglobin vs the surrounding partial pressure of oxygen is shown in Fig. 14. The sigmoidal shape of the oxygen equilibrium curve suggests heme-heme interactions (the cooperativity effect). Upon oxygenation, conformational changes in the molecule have been confirmed by X-ray crystallographic studies.[135]

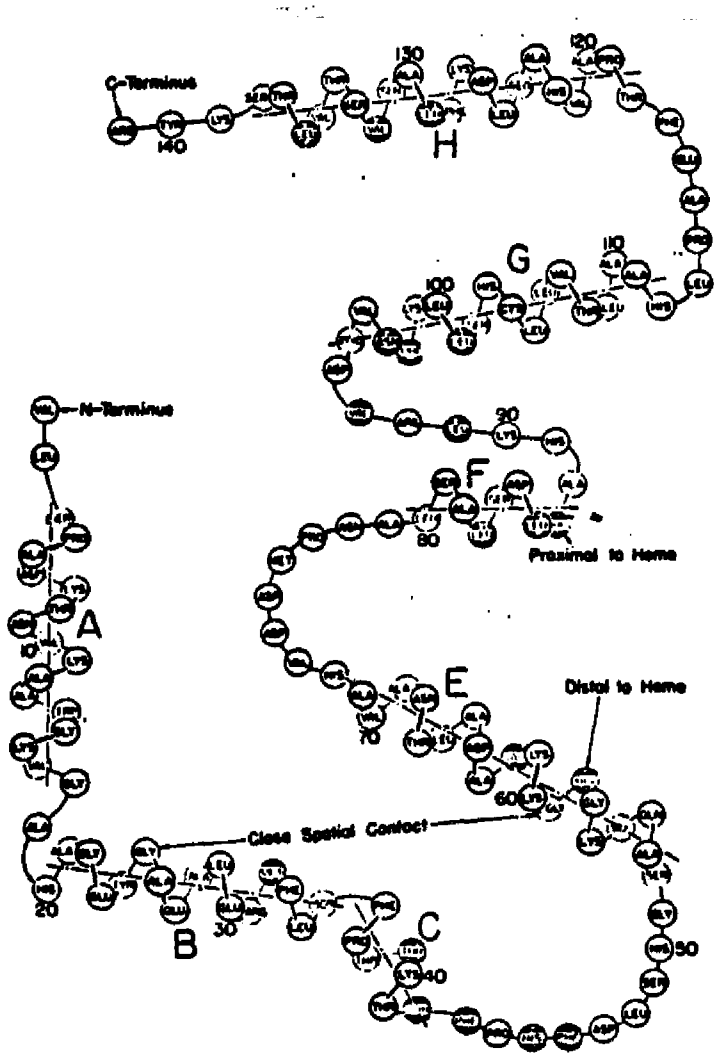

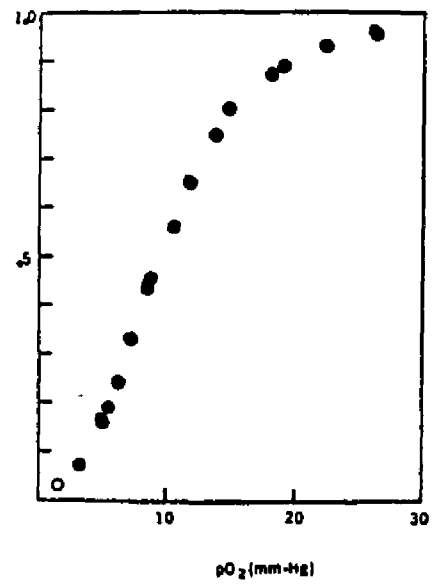

Figure 14
Fraction of oxygen bound to hemoglobin vs. surrounding partial pressure of oxygen.

Figure 13 Amino acid structure of the α-helix of Hemoglobin.

Muirhead and co-workers describe the changes in the relationship of hemoglobin's four chains (upon oxygenation) as that of a screw movement of each along a given reference coordinate system. This movement causes a change in the distance between the iron atoms of the different chains. Perutz showed that in the case of de-oxy hemoglobin, the iron atom is displaced approximately .75 Å normal to the porphyrin ring plane in both α and β chains while lying almost in the plane in the case of oxygenated hemoglobin.[155]

Antonini and Brunori believe that 'movements of this kind appear of importance as a trigger for the more extensive conformation changes associated with ligand binding'.[10] They conclude that the structural changes occur in chains where ligands are bound; these changes are then propagated through interchain contact regions to the other chains thus affecting their affinity for a sixth ligand. Investigations in recent years have shown that the oxygen binding capability of hemoglobin can be influenced by the presence of certain organic phosphates. One of these, 2,3-Diphosphoglycerate (DPG) occurs naturally in significant amounts in the erythrocytes (whole blood cells) of humans as well as other mammalian species.[22,44,176] A specific example of the importance of DPG to hemoglobin is its regulatory effect on oxygen binding at different altitudes.[57,176]

Although the binding site of DPG to hemoglobin is still not known, evidence suggests that DPG binds to deoxygenated hemoglobin in approximately a 1:1 molar ratio or greater.[19,20,65] Investigations suggest that the binding is along the β chains since the isolated α chains (as opposed to the isolated β chains) show little affinity for this (and other) organic phosphates.[19]

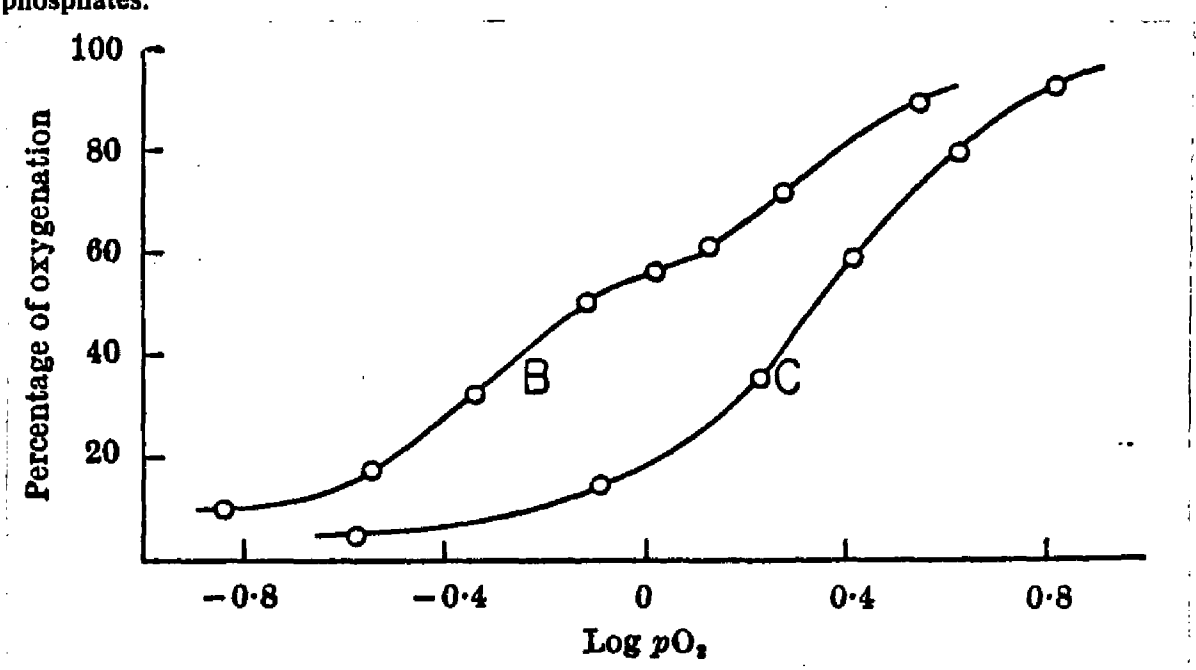

Figure 15 B — hemoglobin; C — hemoglobin with DPG.

Figure 15 shows how the oxygenation curve of hemoglobin is affected by the presence of DPG. DPG probably does not bind to oxyhemoglobin because of steric hindrances present in this conformational state and yet does bind to the deoxy form (one suggestion is that DPG binds in conjunction with the β-chains along the two-fold symmetry axis).[21] One possible explanation for the shift of the oxygen curve is that the presence of DPG acts to prevent the molecular conformational changes necessary to allow 0_2 to bind.[85]

According to the theory proposed by Monot et al.[129] the cooperativity of ligand binding of hemoglobin can be explained in terms of two different quaternary structures: the T structure (low ligand affinity e.g., deoxy hemoglobin) and the R structure (high ligand affinity e.g., oxyhemoglobin). According to Perutz[156] methemoglobin (Fe^{3+}) chains could be stable in either of the high or low affinity forms in a dynamic equilibrium. The fact that methemoglobin binds DPG is well known.[194]

Additionally, Perutz proposes that hemoglobin in solution with pH values close to 6.5 would be in about a 9:1 ratio of R to T configuration. Because DPG binds almost exclusively to the T form of the molecule,[77] Kilmartin suggests that the presence of organic phosphates will shift the equilibrium of the methemoglobin towards the T state (at pH 6.5).[101] Although DPG does not bind in close proximity to the iron atoms, Mossbauer studies were undertaken to determine if a change in the local environment of the iron atom was induced by the presence of DPG on the hemoglobin molecule.

So far we have discussed hemoglobin ligand binding from a semi-macroscopic point of view. From a microscopic point of view, we must discuss the spin-states of the iron porphyrin in both the normal hemoglobin (Fe^{2+}) and methemoglobin (Fe^{3+}) cases. To conclude the discussion of background information about hemoglobin pertinent to our studies, let us describe the atomic nature of the iron environment.

The spin state in the molecule is primarily determined by the 3d iron orbitals. A strong crystal field at the iron may cause a violation of Hund's rule. The field component with cubic symmetry in many cases is much greater than the lower symmetry components, in which case there is a splitting of the iron d orbitals into two groups. In octahedral symmetry, the d_ϵ orbitals are lowest in energy.[107] The delocalization of the iron electrons to the porphyrin ring is small (interaction with the π and σ porphyrin orbitals).[103] The spin quantum number in the Fe^{3+} ion will be 5/2, 3/2, or 1/2 while in the Fe^{2+} ion it will be 2, 1, or 0 depending on the pairing of the iron electrons as influenced by the separation of iron orbitals due to crystal field effects.

When the cubic field component does not cause separation of the d_ϵ and d_γ orbitals of sufficient energy for the electrons to violate Hund's rule, they will occupy all empty orbitals before pairing in the low energy orbitals. This describes what is generally called the 'high spin' state. If however, the field separates the two orbital groups by enough energy and Hund's rule is violated, the electrons will pair in the low energy groups before occupying the higher levels. This state is referred to as 'low spin'. When an atomic configuration leaves a degeneracy of the orbital states, the Jahn-Teller theorem states that the atoms which give rise to the crystal field will arrange themselves so as to lower the symmetry to lift the orbital degeneracy.[94,187] This guarantees field components of low enough symmetries to further split the d_ϵ and d_γ levels.

Since the degeneracy of the d-orbitals is completely removed, the orbital angular momentum will be quenched.[107] The rhombic component of the crystal field is the one which further splits the two previous levels and the 'high spin' and 'low spin' occupation of these for both Fe^{2+} and Fe^{3+} are shown in Fig. 16.[110] In the case of the high spin Fe^{3+} ion, Kramer's theorem tells us that there will still be three levels of 2-fold degeneracy (since 2S + 1 is integer) which can be removed only by an external magnetic field.[104]

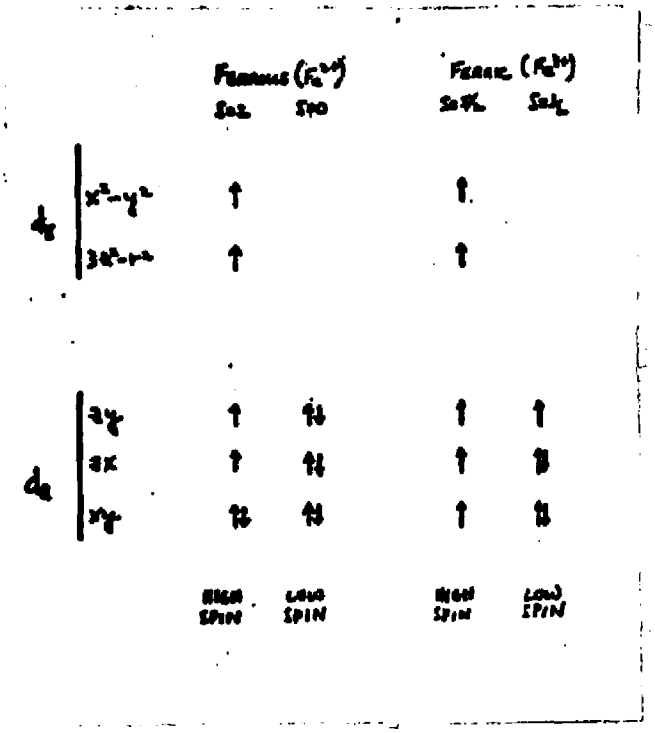

Figure 16 Electron occupation of high and low spin states of Fe^{2+} and Fe^{3+}.

HEMOGLOBIN SAMPLE PREPARATION

To date, most of the hemoglobin studies were made using the protein derived from the whole blood cells of rats[112,194] and humans.[91] In the case of the rats, the animals were made anemic by periodic bleeding and then given Fe^{57} (the isotope necessary for Mossbauer studies) intravenously to increase the percentage of that isotope in their hemoglobin as new red cells were generated. (Fe^{57} occurs with about 2% natural abundance.) In both cases cited, the enrichment of Fe^{57} was judged to be in excess of 50%, while in the case of the human hemoglobin, no enrichment was done. The Mossbauer spectra for both species are similar but no comparative study has been made.

In the unenriched human hemoglobin spectra Huynh et al. report a 1% to 1.5% Mossbauer effect with equipment analogous to that used in our experiments while the enriched rat hemoglobin yielded substantially increased percentage effects.[91] It is well known that rabbits have several genetically distinct forms of hemoglobin and that even for brother and sister, the multiplicity of forms are not constant (these multiple hemoglobins occur in rats as well).[52] Furthermore, relative to human hemoglobin structure, the amino acid differences are numerous. The opposite is the case for the hemoglobin of Rhesus monkeys. Their hemoglobin is about 98% homogeneous (a single genetic form) and there occur only four minor amino acid substitutions (relative to human hemoglobin) in the α and β chains.[52]

For our work, two white albino rabbits were bled from the main artery in the ear every four days for two weeks. In each case, bleeding was stopped when the hematocrit (ratio of whole cell to plasma volume) was about 25 (normal is 38 to 40). After the next four bleedings, 70 mg of Fe^{57} (in the form of iron citrate at pH 6) was injected intravenously (35 mg each rabbit). The rabbits were exanguinated one week later at which time the hematocrit was found to be 38. The whole cells were then hemolysed using distilled water and centrifuged at 17,000 rpm for 1 hour. Two washings followed in .15 molar sodium chloride with a 15 minute centrifuging of 1500 rpm after each. After ultra filtration in an Amicon cell to a concentration

of about .05 milimolar, sodium phosphate buffer at pH 7.2 was added 50:1 in volume to half the sample. The above process was repeated four times; the final solution was concentrated to about 3 milimolar and used to fill ten sample holders of about 1 ml each. The balance of the sample was divided into five groups, each prepared as above but at pH values of 6.9, 7.0, 7.7, 8.0 and 8.2 (two sample holders filled for each pH). The samples were then stored in a nitrogen refrigerator.

A two kilogram female Rhesus monkey was treated much the same as the rabbit regarding the anemia procedure and subsequent iron injections (150 mg. total, Fe^{57} injected). Upon exanguination, about 20% of the whole cells were droplet frozen according to the technique established by Rowe et al.[107]

The balance was bulk frozen in 7 ml ampules according to the same technique. These samples were also put into liquid nitrogen storage and one or two ampules (when needed) would be removed for the preparation of hemoglobin. Oxyhemoglobin samples (at different pH values) were prepared the same way as those of the rabbits. Several sample holders were also filled with the frozen whole cell droplets from the monkey cache. Optical absorption spectra of the rabbit and monkey hemoglobins (at pH 7.2) as well as the whole cell droplets indicated fully oxygenated hemoglobin[10].

HEMOGLOBIN DATA

Oxyhemoglobin, being a low spin Fe^{2+} complex, in the absence of an external magnetic field shows only a simple quadrapole hyperfine split pair typical of those shown in Fig. 17.[191] The Mossbauer percentage effects of the oxyhemoglobin samples ranged between 6.4 and 2.5 over the temperature range from 4° to 163° Kelvin.

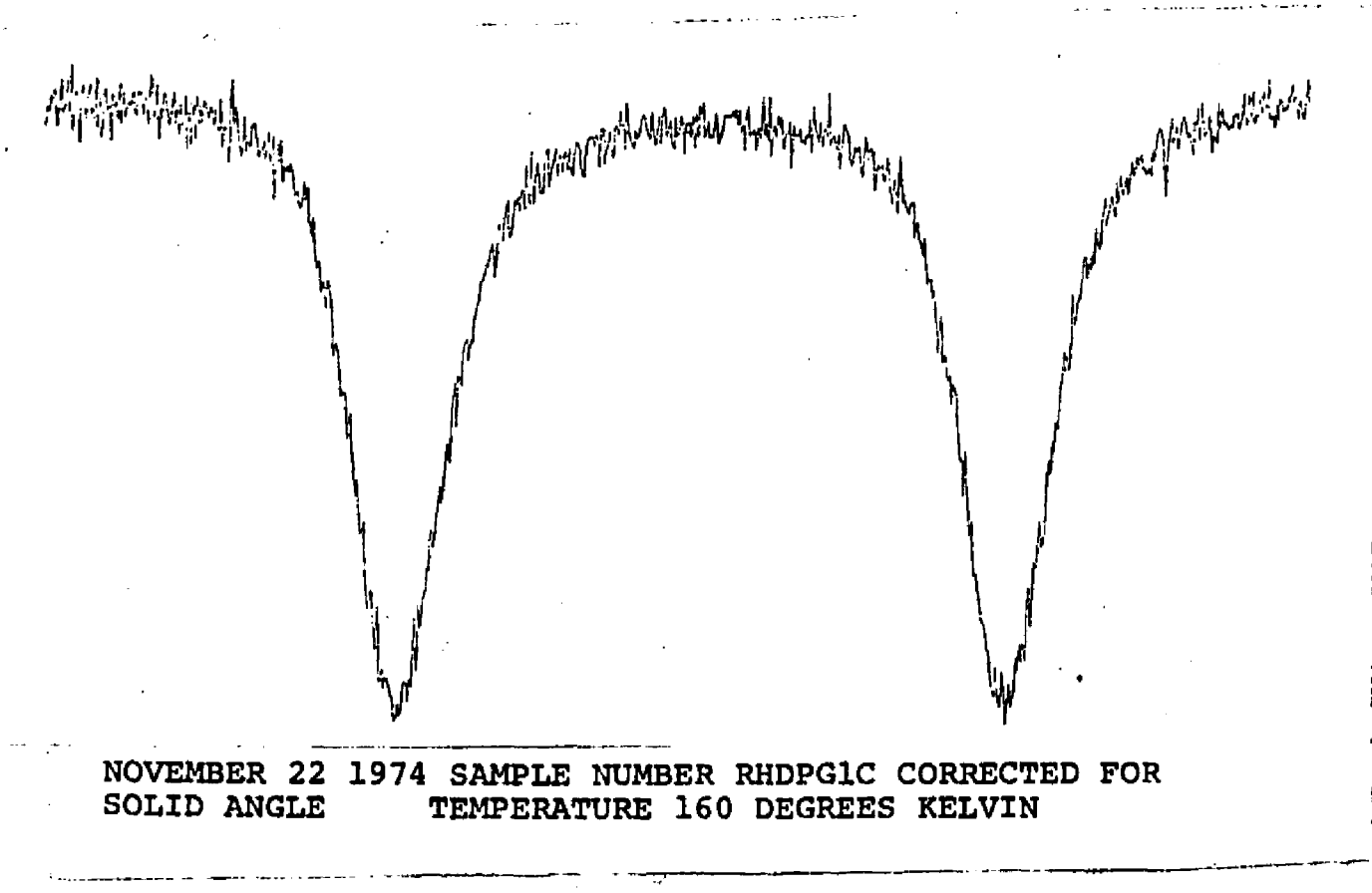

Figure 17 Relative transmission vs. velocity (−3 to +3 mm/sec).

An experiment was conducted to determine if the local iron environment (as seen by the Mossbauer technique) was affected by the differences in the amino acids between the monkey and the rabbits, and another experiment to determine if differences could be measured due to varying the pH values. Two rabbit samples were used, one at a pH of 7.7 and the other at pH 6.9. The monkey oxyhemoglobin was at pH 7.2 and in all cases, the buffer was sodium phosphate in .15 molar sodium chloride. Spectra at 4° Kelvin were accumulated over a period

of about 8 hours. The typical number of counts per channel during this period of time was between 300,000 and 400,000.

The first comparison is that of the rabbit oxyhemoglobins at pH 7.7 (sample RPH77) and pH 6.9 (sample RPH69) at low and high temperatures.

Table 1

pH Dependencies of Rabbit Oxyhemoglobins

		ΔE_q	δ
	Temperature	(quadrapole splitting mm/sec)	(isomer shift mm/sec)
RPH69	4	2.252 ±.003	.299 ±.007
	150-160	1.942 ±.001	.270 ±.006
RPH77	4	2.218 ±.006	.301 ±.003
	150-160	1.922 ±.009	.289 ±.005

The data at 4° Kelvin suggest that there may be differences between these samples. The measured differences of the quadrapole pairs of .034 mm/sec exceeds by a factor of 5 the greatest statistical error measured in a set of samples (i.e., .006 in RPH77). The results in the 150° to 160° range of 1.942±.002 and 1.922±.009 for RPH69 and RPH77 respectively with a measured difference of quadrapole pairs of .020 only exceeds the greatest statistical error by slightly more than a factor of 2. It is well known that the pH of the solvent affects the oxygen affinity of hemoglobin (referred to as the Bohr effect),[10] and while these results do suggest differences in the iron hyperfine splitting, they are not conclusive within the bounds of our experimental accuracies.

Four different Rhesus monkey samples were used for comparative purposes. The first was RH103 which consisted of the untouched frozen droplets of whole blood. RH107 (whole cells only) was prepared from a 7ml batch frozen ampules according to the method of

Rowe et al.[170] RH109 was prepared by hemolysis of a similar preparation of sample RH107 but was washed and put into .067 molar sodium phosphate buffer in isotonic saline before concentration. RHDPGO2 consisted of oxyhemoglobin 'stripped' of DPG by passing it through a Sephadex G-25 column (1.5×45 cm) equilibrated with .067 molar sodium phosphate buffer in .15 molar NaCl.[181] Optical spectra of all samples indicated that the hemoglobin was fully oxygenated. Of the four samples, only RH109 and RHDPGO2 were at a controlled pH of 7.2.

At 4° Kelvin, these monkey samples showed no differences between themselves within the experimentally measured error. They do however exhibit the same differences in quadrapole splittings relative to the rabbit sample at pH 6.9 (RPH69) as did the rabbit sample at pH 7.7 (RPH77). The sample 'stripped' of DPG (RHDPGO2) showed no difference from that which was not (RH109) within the accuracy of our measurements.

Table 2

4° Monkey Oxyhemoglobins

Sample	ΔE_q (quadrapole splitting mm/sec)	δ (isomer shift mm/sec)
RH109 monkey hemoglobin pH 7.2	2.209 ±.003	.289 ±.003
RHDPGO2 monkey hemoglobin pH 7.2 'stripped of DPG'	2.201 ±.004	.303 ±.002
RH107 monkey whole cells	2.207 ±.006	.290 ±.005
RH103 monkey whole cells 'droplets'	2.217 ±.007	.298 ±.008

At higher temperatures the comparisons did show differences between the hemoglobin in and out of the cell.

Table 3

150° to 160° Monkey Oxyhemoglobins

Sample	ΔE_q (quadrapole splitting mm/sec)	δ (isomer shift mm/sec)
RH109 monkey hemoglobin pH 7.2	1.876±.007	.270±.003
RHDPGO2 monkey hemoglobin pH 7.2 'stripped'	1.886±.003	.283±.001
RH107 monkey whole cells	1.903±.002	.270±.001
RH103 monkey whole cell 'droplets'	1.913±.006	.289±.006

The data here is suggestive of quadrapole splittings which differ between about .02 mm/sec and .03 mm/sec for monkey oxyhemoglobin inside and outside the whole cell. These differences are of the order of 3 to 10 times the measured statistical error. Even though susceptibility measurements confirm the diamagnetic state of oxyhemoglobin (confirming a low-spin ferrous state), it has long been experimentally observed that the splitting is large and is strongly temperature dependent.[110] The lower d_ϵ orbitals are completely filled giving rise to cubic symmetry in terms of the electric field gradient contribution of these electrons at the iron nucleus. The ligand charges will be expected to contribute to the EFG but not of sufficient amount to produce the splitting observed. Lang and Marshall argue (Fig. 18) that the large splitting is caused due to the effective reduction of electrons in the d_{yz} orbital due to sharing of these with the π orbitals of the porphyrin ring.[11] The reason that these differences (if real) evidence themselves at higher rather than lower temperatures can readily be justified in terms of temperature dependence of the quadrapole splitting which is yet to be explained.

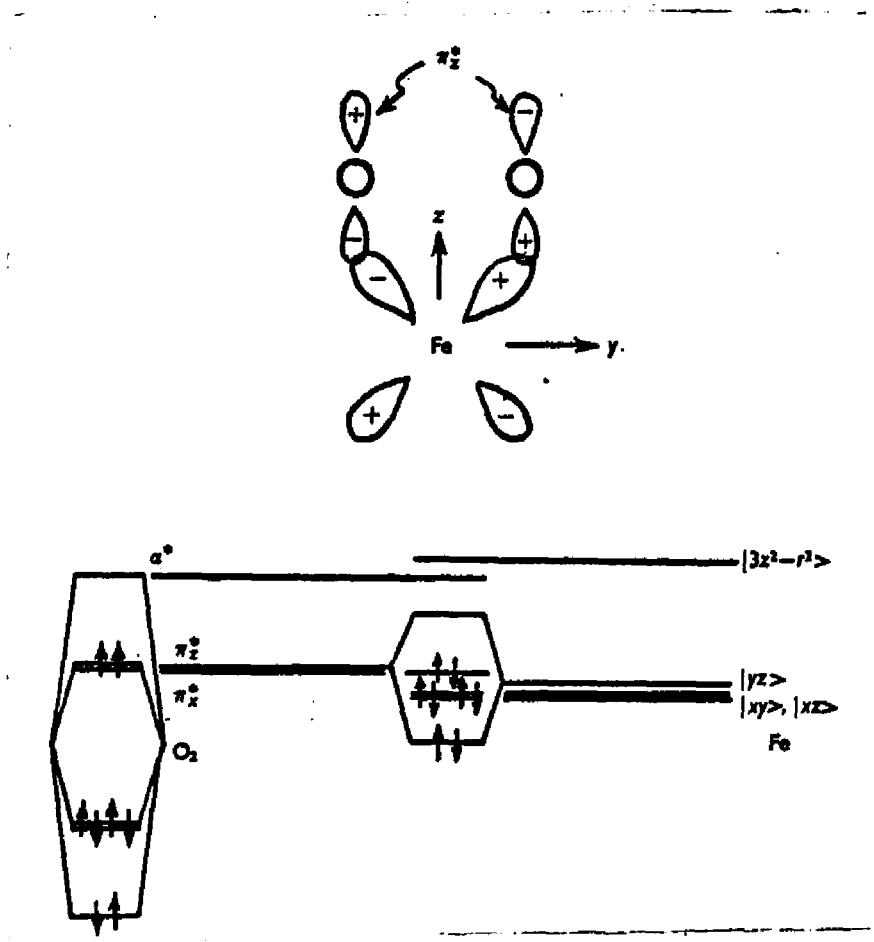

Figure 18 Proposed bonding arrangement and energy levels for oxyhemoglobin.

A reasonable proposal for the temperature dependence of the quadrapole splitting in hemoglobin is that a 'thermally induced vibration or hindered rotation of the oxygen and/or adjacent parts of the protein' may have a charge distribution different from the ground state.[110] A possibility such as this could account for the suggested differences between the species as it is not unreasonable to expect such vibrations or hindrances to depend strongly on the differing environments near the heme. In contrast to the implied differences between the rabbit and monkey spectra, the data is almost conclusive that there are differences in the electric field gradient at the iron nucleus depending on whether the hemoglobin is in or out of the cell. This seems reasonable in view of the probable differences in conformational structure of the proteins due to the environmental differences in and out of the whole red blood cell. It is also possible that upon removal from the whole blood cell, DPG which may have been bound to the hemoglobin in that environment due to high levels in the cell may have been

disassociated from the molecule during dilution and subsequent re-concentration during preparation. Thus, a contributory cause of the observed differences of hemoglobin in and out of the whole cell may be due to DPG binding to the molecule.

μ-OXO-BIS PORPHYRIN COMPLEXES

In the case where the iron porphyrin complex is embedded in a large molecule, there are many subtle effects contributing to the behavior of the iron atom (e.g. conformational changes in molecular structure). By studying the porphyrin complex as a separate entity, we hope to better understand the effects of the local environment upon the iron. One class of porphyrin complexes which has been the subject of recent study is that in which two iron porphyrins form dimers via a bridging oxygen atom. These μ-oxo-bis complexes have further been found to have the iron atoms anti-ferromagnetically coupled.[131,192]

The full understanding of the chemical nature of these complexes is important because this type of antiferromagnetic coupling is believed to exist in several proteins of biological importance such as cytochrome oxidase.[140]

A study of six of these complexes was made by the method of Mossbauer spectroscopy in order to correlate with data already available by other techniques.

Figure 12 showed the basic porphyrin complex with the vinyl groups situated at the 2,4 positions on the pyrrole ring. The μ-oxo-bis dimer of this porphyrin (Fe^{3+}), the meso and deutero porphyrins (ethyl groups and hydrogen atoms at the 2,4 positions respectively) as well as three other substituted variations were those used for the studies of O'Keefe at al.[140]

The six samples (with our aliases following the ':') were:

1. μ-oxo-bis (protohemin dimethyl ester) : PROTO
2. μ-oxo-bis (mesohemin dimethyl ester) : MESO
3. μ-oxo-bis (deuterohemin dimethyl ester) : DEUTERO
4. μ-oxo-bis (2,4-dipropionyl deuterohemin dimethyl ester) : DIPROPIONYL
5. μ-oxo-bis (2,4-diacetyl deuteroheim dimethyl ester) : DIACETYL
6. μ-oxo-bis (2,4-di(2′-ethoxycarbonyl) cyclopropyl deuterohemin dimethyl ester) : CYCLO-PROPYL

The preparations of these lypholized samples is discussed by O'Keefe et al.[140]

Mossbauer studies of these complexes confirm the change of the electronic environment as a function of the 2,4 substituents on the porphyrin ring and will be presented and discussed in view of other accumulated data. The most interesting finding with regard to these complexes is the observation of a well defined temperature dependent anisotropy in the recoilless-Mossbauer fraction (the so called Gold'anskii-Karyagin effect); hereafter referred to as the GKE.[71]

μ-OXO-BIS PORPHYRIN DATA

All spectra were accumulated for each sample at various temperatures between 4° and 293° Kelvin. At 4° Kelvin, a weak external magnetic field (600 gauss) confirmed the diamagnetic properties of these samples, i.e., no further hyperfine splitting was observed.

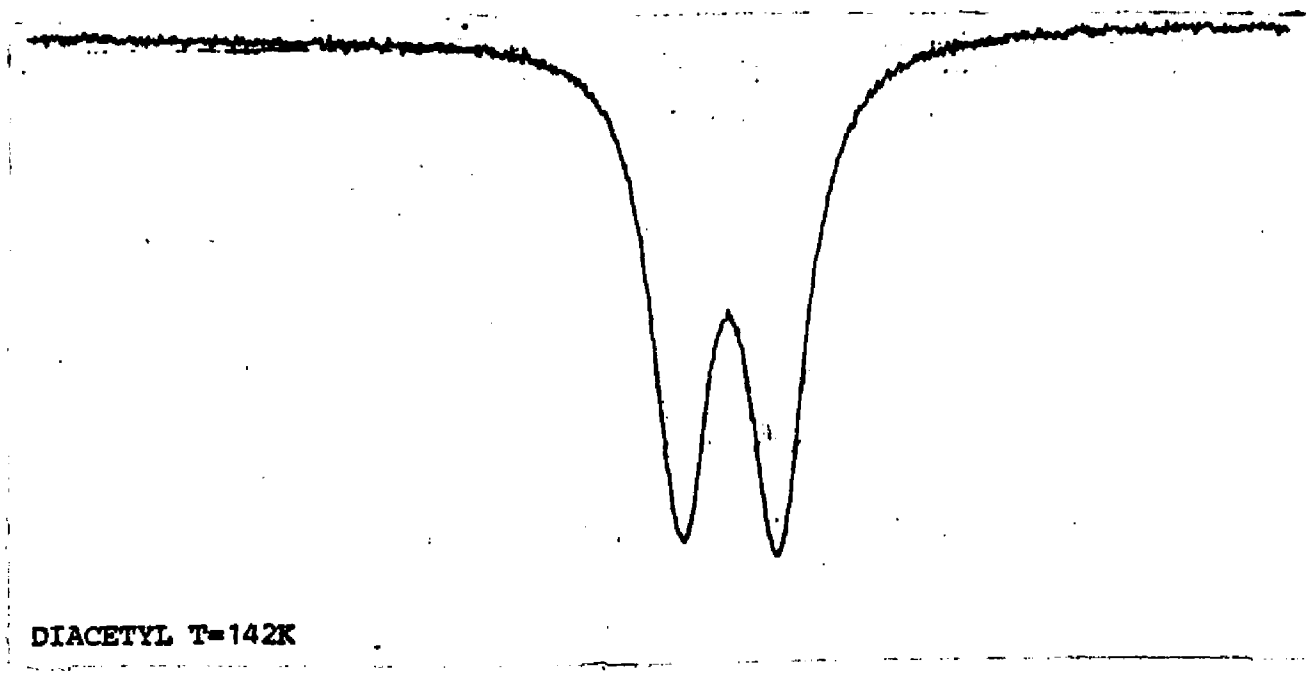

Figure 19 Relative transmission vs. velocity (−3 to +3 mm/sec).

The quadrapole splittings, ΔE_q (the separation between the two minima) and the isomer shift, δ (the displacement of the center of gravity of the spectra relative to that of our iron foil standard) as determined by a computer least squares fit of the data for all six samples is presented below. The spectra are all typical of the one shown in Fig. 19.

Table 4

4° to 293° μ-oxo-bis Complexes

Sample	Temperature(°K)	ΔE_q(mm/sec)	δ(mm/sec)
DIACETYL	4	.387	.431
	142	.407	.406
	159	.403	.402
	293	.394	.297
DIPROPIONYL	4	.433	.431
	143	.430	.408
	293	.419	.293
PROTO	4	.442	.425
	142	.436	.403
	157	.432	.391
	293	.413	.295
MESO	4	.515	.436
	146	.549	.409
	159	.546	.405
	293	.527	.295
CYCLOPROPYL	4	.560	.440
	139	.552	.423
	144	.554	.418
	293	.545	.296
DEUTERO	4	.577	.448
	141	592	.427
	160	.593	.412
	293	.579	.310

CORRELATION WITH OTHER DATA

Magnetic susceptibility studies of all but the Fe^{2+} protheme complex fit a dimeric model of two antiferromagnetically coupled spins of 5/2. O'Keefe et al. have calculated both the antiferromagnetic coupling constants (J) which are listed below along with the infra-red vibration of frequencies (ν) attributed to the Fe-O-Fe bond.

Table 5

Antiferromagnetic Coupling Constants and Infra-red Vibration Frequencies of μ-oxo-bis Porphyrin Complexes

Sample	J, °K±5°K	$\nu_{cm}^{-1} \pm 1.0 cm^{-1}$
DIACETYL	205	886
DIPROPIONYL	205	882
PROTO	190	880
MESO	210	885
CYCLOPROPYL	195	884
DEUTERO	175	842

The Fe-O-Fe bond angles for all these complexes are in the range of 170° to 180° according to O'Keefe et al. with the angle increasing as the antiferromagnetic coupling constant increases. Additionally, the electronic absorption spectra in the 3000Å to 12000Å region for these six complexes in benzene yield wavelength and extinction values for band maxima shown in Table 6.[140]

Table 6

Electronic Absorption Data of μ-oxo-bis Porphyrin Complexes

	$\lambda_{max,nm}(A_{mM})$	$\lambda_{max,nm}(A_{mM})$	$\lambda_{max,nm}(A_{mM})$	$\lambda_{max,nm}(A_{mM})$
DIACETYL	626(8.2)	582(13.9)	415(95.5)	341(63.2)
DIPROPIONYL	626(7.7)	580(13.8)	415(94.8)	340(61.3)
PROTO	599(11.8)	573(14.1)	397(115)	357(75.2)
MESO	590(11.0)	564(13.4)	389(121)	343(80.2)
CYCLOPROPYL	592(12.0)	568(15.0)	393(117)	344(75.7)
DEUTERO	584(10.1)	563(12.9)	390(120)	334(68.7)

The interaction (in the absence of external magnetic fields) of the electric field gradient with the nuclear quadrapole moment will be influenced by the withdrawal of d-electrons to the porphyrin ring in two ways. To first order the five electrons in a d-orbital (high-spin) constitute a half-filled shell, and they will yield a zero-electric field gradient at the nucleus.[49] However, partial removal of d-electrons by the porphyrin ring will cause an asymmetric d electron density. This asymmetric spatial distribution of charge will polarize the inner spherically symmetric shells resulting in an electric field gradient at the nucleus of opposite sign to that caused by the unbalanced charge of the ionic electrons. Introducing **R** as shielding factor ($0<\mathbf{R}<1$), the EFG due to the ion itself will be reduced by a factor of $1 - \mathbf{R}$.

The surrounding lattice can also contribute to the electric field gradient at the nucleus and the non-uniform charge distribution which is the basis for this will also cause a polarization of the inner shell electrons. The term γ_∞ is used by convention (the Sternheimer anti-shielding factor) to modify the contribution of the lattice EFG by a factor of $1 - \gamma_\infty$. This effect may be positive or negative and $|\gamma_\infty|$ can be as large as 100.

$$\text{Thus } \Delta E_q \alpha V_{zz} = (1-R)V_{zz}^{ion} + (1-\gamma_\infty)V_{zz}^{lattice} \quad (9)$$

where **R** and γ_∞ are shielding and anti-shielding coefficients described.

Covalency between the iron and the coupling oxygen atom must also be considered as a d-orbital electron reduction factor. This type of superexchange coupling between ions with half filled orbitals is consistent with magnetic data for a linear system.[74]

Covalency between the iron atom and the porphyrin may be considered a measure of the 'electron withdrawing power' or basicity of the porphyrin, and since in our complexes we are changing the 2,4 substituents, the basicity of the porphyrin as a function of the electron withdrawing power of its side chains is of importance. A quantitative measure of electron withdrawing power of the porphyrin ring can be defined by its pK values.

According to the convention of Phillips we define[158]

$$pK_1 = pH\text{-}\log[P^{2-}]/[PH] \quad (10)$$

$$pK_2 = pH\text{-}\log[PH^-]/[PH_2] \quad (10a)$$

$$pK_3 = pH\text{-}\log[PH_2]/[PH_3^+] \quad (10b)$$

$$pK_4 = pH\text{-}\log[PH_3^+]/[PH_4^{2+}] \quad (10c)$$

where the different neutral, anionic and cationic forms of porhin are shown in Fig. 20.

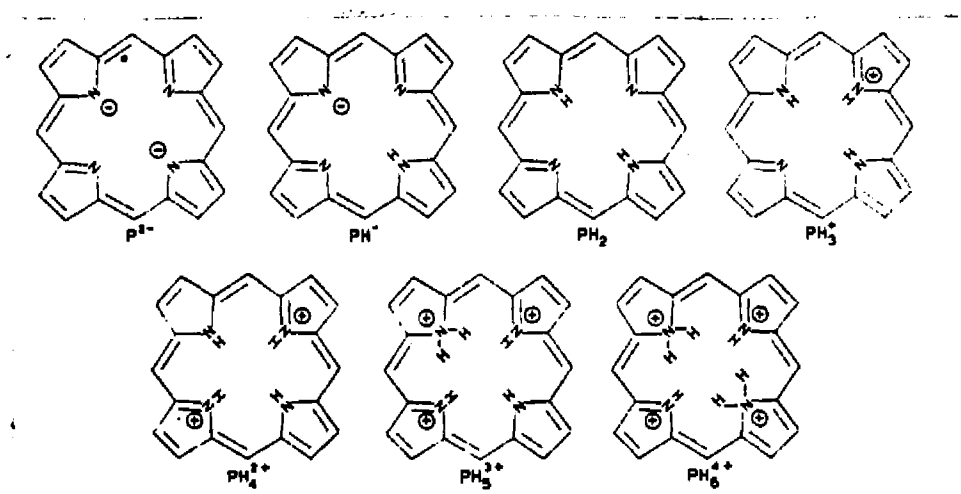

Figure 20 Neutral, anionic and cationic forms of porphin.

While pK_1 and pK_2 values refer to acidic equilibria (of proton removal from the pyrrole nitrogens), the pK_3 and pK_4 values refer to addition of protons to the pyrolenine nitrogens. The addition of the first proton ($PH_2 + H^+ \rightarrow PH_3^+$) is determined by the pK_3 and the values for our six complexes are as follows:[38]

Table 7

pK_3 Values of μ-oxo-bis Porphyrin Complexes

COMPLEX	$pK_3 \pm .01$
DIPROPIONYL	3.2
DIACETYL	3.3
PROTO	4.8
CYCLOPROPYL	4.8
DEUTERO	5.5
MESO	5.8

A single hydrogen at each of the 2,4 positions will lower the basicity of the porphyrin due to its strong electron attracting powers.

The covalency between porphyrin as determined by the pK_3 values will then (to a first order approximation) account for the increasing values of ΔE_q in going from DIACETYL to DEUTERO.

Table 8

pK_3 and Temperature Dependent Quadrapole Splitting
of μ-oxo-bis Porphyrin Complexes

	$pK_3 \pm .01$	$\Delta Eq(4°K; mm/sec)$	$\Delta Eq(293°K; mm/sec)$
DIACETYL	3.3	.387	.394
DIPROPIONYL	3.2	.433	.419
PROTO	4.8	.442	.413
MESO	5.8	.515	.527
CYCLOPROPYL	4.8	.560	.545
DEUTERO	5.5	.577	.579

However, we clearly see that the ethyl substituents (MESO) strongly violate this approximation. O'Keefe et al. have noted that with the exception of the MESO complex, a plot of the J (antiferromagnetic coupling constant) values vs. the pK_3 shows a trend toward weaker iron-axial ligand interaction consistent with increasing iron-porphyrin interaction.[140]

Table 9

pK_3 and antiferromagnetic coupling constants
of μ-oxo-bis porphyrin complexes

COMPLEX	$pK_3 \pm .01$	$J°K \pm 5°K$
DIPROPIONYL	3.2	205
DIACETYL	3.3	205
PROTO	4.8	190
CYCLOPROPYL	4.8	195
DEUTERO	5.5	175
MESO	5.8	210

They further argue that as the Fe-O-Fe bond angle approaches 180°, symmetry considerations can become dominant enough to override weak iron-ligand coupling, and the Fe-O-Fe bond angle will be roughly proportional to the infra-red vibrational frequency with the smallest angle assigned to the deutero-porphyrin.

The Mossbauer data suggest that a possible correlation of these other data lies in the fact that as the Fe-O-Fe bond angle changes, so does the crystal field contribution to the EFG. The iron is displaced away from the porphyrin plane by about .4 Å in these types of complexes.[117] It is not unreasonable to expect a change in the crystal field contribution to the EFG as the iron-porphyrin ring separations change. Small perturbations in the Fe-O-Fe angle could certainly account for this effect. As a second order correction to the dependence of ΔE_q vs. pK_3 then, increasing value of J would imply a lowering of the crystal field contribution to the EFG (relative to some maximum). The binding strength between the iron and the oxygen contributes mainly to the covalent part of the EFG while further displacement of the iron from the plane of the porphyrin will lower the symmetry of the crystal field (thus affecting that part of the EFG contribution).

The small temperature dependence of the quadrapole splitting is consistent with theoretical variations due to a Boltzman population of electronic states contributing to the valence EFG.[80] Furthermore, the greatest deviation over the measured temperature for any sample is .034 mm/sec (for the MESO complex) while the smallest is .014 (for the DIPROPIONYL). These differences are comparable to those observed by Torrens et al. in their studies of μ-oxo-bis [α,β,γ-δ-tetrakis (aryl, pyridyl and thienyl) porphinatoiron (III)] complexes.[183]

The overall differences in the quadrapole splittings from one complex to another (e.g., .046, .009, .073, .045, .017 mm/sec) going from diacetyl to deutero at 4°K are most probably due to extremely small differences in their crystal fields. It is interesting that the overall difference in ΔE_q among the six complexes is less than .2 mm/sec over the entire range of

temperatures. The fact that the MESO complex has a smaller than expected quadrapole splitting (based on its basicity relative to DEUTERO) is not unreasonable since its magnetic coupling constant is indicative of the higher symmetry of its surroundings, hence a smaller partial contribution to the splitting. The outstanding difference is the comparable values from J and pK_3 for the vinyl and cyclopropyl groups (PROTO and CYCLOPROPYL). It is reasonable that the bulky cyclopropyl group inflicts steric hindrances to the dimer, causing a lowering of the symmetry of the crystal field; hence the greater splitting relative to PROTO.

TEMPERATURE DEPENDENT ASYMMETRIES

All of the dimeric samples studied exhibited to some degree a temperature dependent asymmetry of the simple quadrapole resonance absorption peaks. Three sample spectra are shown in Fig. 21 of the proto-porphyrin complex. As a general rule, as the magnitude of the quadrapole splitting increases (from one sample to another), the asymmetry of the intensities decreases.

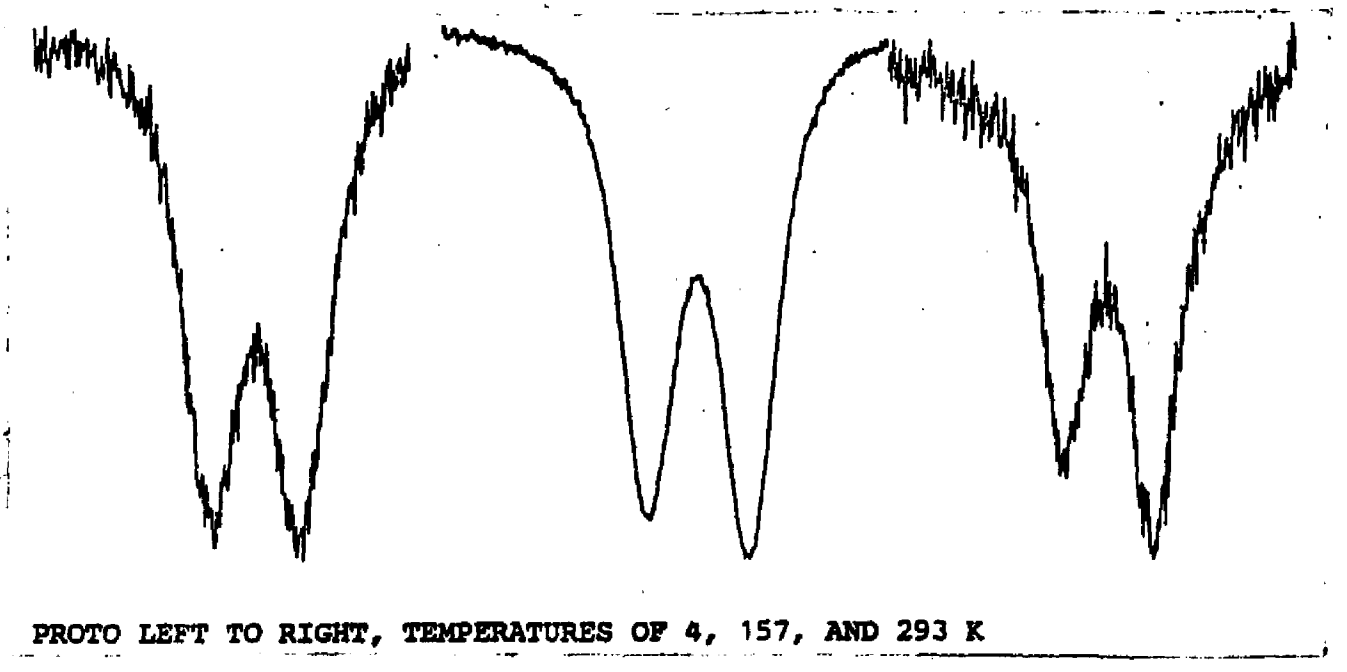

Figure 21 Relative transmission vs. velocity (−1 to +1.5 mm/sec).

In order to understand the physics of the observed asymmetries, it is necessary to discuss all possible causes. The first is typified by Fig. 22 and is that of acetatodeutero porphyrin IX dimethyl ester iron III at 293°K.[132]

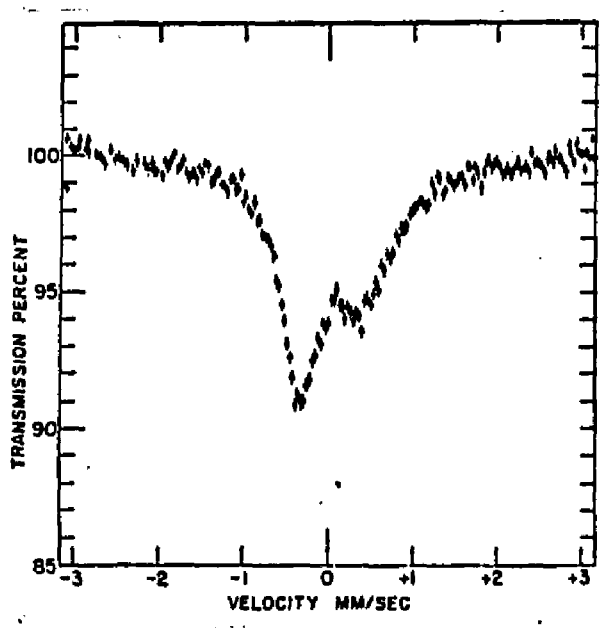

Figure 22 Mossbauer spectrum of acetatodeutero porphyrin IX dimethyl ester.

This asymmetry effect is due to the fact that the electron spin relaxation is slow compared to the lifetime of the excited nuclear state. Thus, there is an effective magnetic field (from the electronic moments) at the nucleus which will remove the degeneracy of the $M_I = \pm 3/2$ and $M_I = \pm 1/2$ excited states. The nuclear precession frequency in the non-zero electronic field is larger for the $M_I = \pm 3/2$ to $M_I = \pm 1/2$ state.[24]

Spin-spin interactions can also cause an asymmetry. This effect will be dependent on paramagnetic ion concentration but will essentially be temperature independent.[24] The presence of two different iron environments could also cause an apparent asymmetry as well as a single line impurity which overlaps either resonance line.[66]

None of the causes listed so far are substantiated by our data, leaving only two other possibilities. The transition probabilities (which determine the intensities) are a function of the angle Θ between the γ-photon beam and the principal axis of the electric field gradient.

The angular dependence of the ratio of the transition probabilities[49] is $(1 + \cos^2\Theta)/(5/3-\cos^2\Theta)$.

Although the ratio of the two transition probabilities averages to 1 over the range $0 \leq \Theta \leq \pi$ (which is the case for a randomly oriented absorber), the ratio is not in general unity for a fixed angle. Using the convention of Gold'anskii and Markarov[71] we refer to $\pm 3/2$ to $\pm 1/2$ transitions and $\pm 1/2$ to $\pm 1/2$ transitions as $M_{3/2 \rightarrow 1/2} = M_{\pi}$ and $M_{1/2 \rightarrow 1/2} = M_{\sigma}$ respectively.

Thus for $\Theta = 90°$, $(M_{\sigma} / M_{\pi}) = 3/5$. While for $\Theta = 0°$, $M_{\sigma} = M_{\pi} = 1/3$. It is clear then, if a powered crystalline sample is not truly random but rather has partial orientation, that an experimentally introduced asymmetry will appear. This was exactly the effect in Di-iron Enneacarbonyl reported erroneously by Gibb et al.[67] and then later explained.[66] In their later paper, Gibb et al. report the only way to insure total random orientation is to grind thoroughly the sample with an abrasive powder such as Al_2O_3 or quartz glass.

The last of the possible causes of the asymmetry is due to the fact that the rms vibrational amplitudes of the Mossbauer atom are not isotropic. Our initial spectra were taken with no alteration of the original sample preparation. Later, new spectra were gathered for each sample after grinding with powdered quartz glass. These results indicated no differences in the measured asymmetry.

Since the Mossbauer fraction depends on the rms atomic displacement, we can for example in the case of axial symmetry construct a theoretical model for the temperature dependent asymmetry.

$$\text{Let } (X_{\perp}^2) = (X_x) = (X_y^2) \tag{11}$$

$$(X_{\parallel}^2) = (X_z^2) \tag{11a}$$

and

$$(X_{\perp}^2) \neq (X_{\parallel}^2), \tag{11b}$$

then it can be shown that at a fixed temperature[72]

$$\frac{M_{\sigma}}{M_{\pi}} = \frac{(\int_0^{\pi} \exp[-(1/\lambda^2)\{(X_{\parallel}^2) - (X_{\perp}^2)\}\cos^2\Theta](1 + \cos^2\Theta)\sin\Theta \, d\Theta)}{(\int_0^{\pi} \exp[-(1/\lambda^2)\{\langle X_{\parallel}^2\rangle - \langle X_{\perp}^2\rangle\}\cos^2\Theta]\sin\Theta \, d\Theta)}. \tag{12}$$

The spectral data were fitted by least squares to 2 Lorentzian lines of width Γ_+ and Γ_- (where the + and − subscripts refer to the higher and lower velocities respectively). Since we are dealing with the ratio of the integrated intensities, we define (for each absorption curve) the quantity $I = (I_\infty - I_{min})\Gamma$ where I_∞ is the intensity of the curve where no effect is observed (the baseline), I_{min} is the intensity of the minima, and Γ is the fitted linewidth. Thus the quantities

$$I_\pm = (I_{\pm\infty} - I_{\pm min})\Gamma_\pm$$

define the integrated intensities for the higher and lower velocity peaks respectively.

For each absorption curve, we can also define the % effect as

$(I_\infty - I_{min})/I_\infty$.

Using the convention $R = I_+/I_-$ the measured data for the asymmetry are as follows:

Table 10

Temperature Dependencies of Asymmetries of μ-oxo-bis Complexes

Sample	Temperature (°K)	% Effect	$R=I_+/I_-$
DIACETYL	293	3.6	1.117
	159	9.5	1.023
	142	19.6	1.017
	4	15.2	1.042
DIPROPIONYL	293	2.8	1.197
	143	10.0	1.069
	4	14.9	1.008
PROTO	293	3.9	1.182
	157	12.4	1.080
	142	14.5	1.013
	4	20.2	1.022
MESO	293	2.3	1.089
	159	5.8	1.021
	148	7.5	0.993
	142	7.5	1.015
	4	8.6	1.024
CYCLO	293	1.0	1.044
	144	6.9	0.978
	139	7.5	0.982
	4	12.9	0.971
DEUTERO	293	3.7	1.003
	160	14.0	0.968
	141	15.0	0.981
	4	20.0	1.008

The % effect is relative to the baseline count and represents the average of the two peaks in each case. In these studies and in the following text, these values are used only as guidelines. Because the exact quantity of each sample measured was not the same, the experimental fractions observed cannot be used to determine absolute relative percentage effects between them. The room temperature data exhibit the greatest asymmetry and all samples tend toward a value of unity as the temperature approaches 0° Kelvin. The degree of measured asymmetry will depend upon the difference between the transverse and longitudinal rms atomic amplitudes.

The Mossbauer fraction as given by theory is[186]

$$f = \exp\{-(1/\lambda^2) <(\mathbf{i}\mathbf{X})^2>\} \tag{13}$$

where $\mathbf{i}$ is a unit vector in the direction of the incident γ-ray beam.

For a Debye solid, (an isotropic elastic medium in which lattice vibrations range from frequencies of $0 \leq \omega \leq \omega_{max}$) the expression for the Mossbauer fraction is well known and is given by[63]

$$\exp[(-6E_R/k_b\Theta_d)\{1/4 + (T/\Theta_d)^2\int_0^{\Theta_d/T} u\,du/(e^u-1)\}] \tag{14}$$

where $\Theta_d = \hbar\omega_{max}/k_b$, and E_R is the recoil energy.

The shortcomings of the Debye approximation for a solid (especially at temperatures far from 0°K) are well known.[107] In anisotropic solids where the unit cell is not monatomic, the expression for the Mossbauer fraction must be carefully derived. A first approximation is to include in Eq. 13 for the vector X the fact that it represents the sum of acoustical (continuous frequencies) and optical (discrete frequencies) contributions, e.g.,

$$\mathbf{X} = \mathbf{X}_{acc} + \mathbf{X}_{opt}. \tag{15}$$

The Mossbauer fraction calculated from a purely optical (Einstein) model has the form[191]

$$\exp\left[-(E_R/\hbar\omega_0)\coth(\hbar\omega_0/2k_bT)\right] \tag{16}$$

where ω_0 is the characteristic vibrational frequency of the solid.

In complicated molecular crystals (such as those investigated here) where the unit cell contains atoms of many kinds, an exact expression for the Mossbauer fraction in terms of the crystal parameters would require a precise model of the crystal, however, the assumption that the vibrations consist of two types, high frequency (optical) modes of the atoms in a molecule and low frequency (acoustical) molecular vibrations, is reasonable.[97]

Expressing the total Mossbauer fraction as the product of both contributions, one gets

$$f = f_{acoustical}f_{optical} \tag{17}$$

where for the acoustical contribution, one must be careful to use the mass of the entire vibrating molecular unit. The justification for the separation of these two contributing factors lies in the fact that in general the inter-molecular bonding forces (such as Van der Waals) are several orders of magnitude less than those which bind the atoms within the molecules.[71]

Anisotropic nuclear vibrations in a molecule and/or molecular vibrations in a crystal lead to an asymmetric intensity of the quadrapole hyperfine spectrum, an effect (GKE) named for those who first predicted it theoretically, Gold'anskii and Karyagin.

$$i_x = \sin\theta\cos\varphi, \qquad i_y = \sin\theta\sin\varphi, \qquad i_z = \cos\theta$$

$$\langle(ix)^2\rangle = [\langle x_x^2\rangle\cos^2\varphi + \langle x_y^2\rangle\sin^2\varphi]\sin^2\theta + \langle x_z^2\rangle\cos^2\theta$$

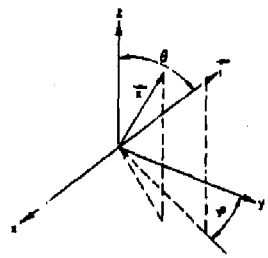

Figure 23 Positions of vectors X and i relative to coordinates x, y, z.

In Fig. 23, referring to equation 13, let Θ represent the angle between the EFG and the X-ray quanta incident on the iron nucleus. Then assuming the EFG and molecular Z axis coincide, we can write $i_x = \sin\Theta\cos\phi$, $i_y = \sin\Theta\sin\phi$ and $i_z = \cos\Theta$, therefore,

$$\langle iX^2\rangle = [\langle X_x^2\rangle\cos^2\phi + \langle X_y^2\rangle\sin^2\phi]\sin^2\Theta + \langle X_z^2\rangle\cos^2\Theta. \tag{18}$$

For axial symmetry,

$$\langle X_x^2\rangle = \langle X_y^2\rangle \text{ and } \langle iX^2\rangle = \langle X_\perp^2\rangle + [\langle X_\parallel^2\rangle - \langle X_\perp^2\rangle]\cos^2\Theta \tag{19}$$

According to Gold'anskii and Makarov the function for the Mossbauer fraction is now[71]

$$f'(\Theta) = \exp\{-\langle X_\perp^2\rangle/\lambda^2\} \quad \exp\{-(\langle X_\parallel^2\rangle - \langle X_\perp^2\rangle)\cos^2\Theta/\lambda^2\}. \tag{20}$$

The ratio of the two intensities can be written as

$$A = \frac{M_\pi}{M_\sigma} = \frac{\int f'(\Theta)(1+\cos^2\Theta)\sin\Theta d\Theta}{\int f'(\Theta)(5/3-\cos^2\Theta)\sin\Theta d\Theta} \tag{21}$$

or

$$A = \frac{\int_0^\pi\{\exp(-N\cos^2\Theta)\}(1+\cos^2\Theta)\sin\Theta d\Theta}{\int_0^\pi\{\exp(-N\cos^2\Theta)\}(5/3-\cos^2\Theta)\sin\Theta d\Theta} \tag{21a}$$

where $N = 1/\lambda^2[\langle X_\parallel^2\rangle - \langle X_\perp^2\rangle]$ (21b)

An estimate of the magnitude of the asymmetry contribution due to the effect of the differences in transverse and longitudinal rms positional uncertainties has been worked out by Kagan for a simple lattice of the rhombic system based on nearest neighbor interactions.[97,99] He predicts an anisotropic Mossbauer effect which will be determined by the elements of a tensor T^{ii} whose principal axis lies along the crystal axis. The diagonal elements of this tensor are given by

$$T^{ii} = (R/2k_bT) \int_0^\infty \exp\{(-\hbar^2/2m(kT)^2 (\sum_{\alpha=1}^{3} \gamma_{i\alpha})t\} \Theta(t) \prod_{\alpha=1}^{3} (I_0 (\hbar^2\gamma_{i\alpha}t/2m(kT)^2)dt \qquad (22)$$

where $\Theta(t)$ is the Jacobi function of the third kind with argument of $i\pi t$, and the matrix elements $\gamma_{\alpha\beta}$ are related to the elastic constants of the crystal.

One would like to present a simple model based on reasonable assumptions which could explain in a semi-quantitative way the temperature dependence of this asymmetry. We begin with a three-dimensional simple harmonic oscillator whose spring constants in the x-y plane are equal and lie along the x-y axes and a different spring constant along the z axis.

To first order, we can consider the vibrations in the x-y plane and perpendicular to the x-y plane as independent. Using the convention $\perp$ as meaning perpendicular to the z axis (i.e., in the x-y plane) and $\parallel$ as meaning along the z axis, the average energy of the oscillator in each direction will be

$$\langle E\rangle_\perp = 2m\omega_\perp^2 \langle X_\perp^2\rangle = 2\hbar\omega_\perp (1/2 + 1/(e^{\hbar\omega_\perp/kT} - 1)) \qquad (23)$$

$$\text{and } \langle E\rangle_\parallel = m\omega_\parallel^2\langle X_\parallel^2\rangle = \hbar\omega_\parallel(1/2 + 1/(e^{\hbar\omega_\parallel/kT} - 1)) \qquad (23a)$$

which gives

$$\langle X_\perp^2\rangle = (\hbar)/(m\omega_\perp) \coth(\hbar\omega_\perp)/(2kT) \qquad (24)$$

$$\langle X_\parallel^2\rangle = (\hbar)/(m\omega_\parallel) \coth(\hbar\omega_\parallel)/(2kT) \qquad (24a)$$

This approximation suggests two realistic frequencies ($\omega_\perp$ and $\omega_\parallel$) for which this simple model could roughly account for the observed asymmetry in terms of the rms deviations of the coordinate positions.

It is simple to calculate from this model the values $\langle X_\parallel^2\rangle - \langle X_\perp^2\rangle$, $\langle X_\parallel^2\rangle/\langle X_\perp^2\rangle$, $\langle X_\parallel^2\rangle^{1/2}$ and $\langle X_\perp^2\rangle^{1/2}$, for any temperature. In tin-dimethyl fluoride, Herber and Chandra have measured I_+/I_- at 294°K, 78°K and 9°K as .78, 1.05 and 1.05 respectively.[84] X-ray data have yielded room temperature bond distances along and perpendicular to the z-axis of 2.12Å and 2.08Å with rms deviations $\langle X_\perp^2\rangle$ = .137Å and $\langle X_\parallel^2\rangle$ = .210Å respectively which are of the order of 1/10 the bond distances at this temperature.[172]

Equation 21a can be numerically integrated with N as a parameter and thus a value of the asymmetry can be predicted as a function of $\langle X_\parallel^2\rangle - \langle X_\perp^2\rangle$. Based on the X-ray data, Eq. 21a yields (at 294°K) a value of .72 which is in reasonable agreement with its measured value of .78. In our model, we shall calculate $\langle X_\parallel^2\rangle$ and $\langle X_\perp^2\rangle$ as per Eqs. 24 and 24a as functions of temperature, and by substituting $\langle X_\parallel^2\rangle - \langle X_\perp^2\rangle$ into 21a and 21b, determine values for asymmetry which we can compare with the observed effect. The next step is then to estimate reasonable values of $\omega_\perp$ and $\omega_\parallel$ based on experimental evidence.

For μ-oxo-bis [protohemin dimethyl ester] X-ray data indicate an in-plane Fe – N average bond distance of 2.08Å and an Fe – O bond distance of 1.73Å.[140] Before estimating the proper vibrational frequencies, it is informative to investigate the rms deviations of the positional coordinate based on Eqs. 24 and 24a.

Figure 24 shows a plot of $\langle X^2\rangle$ vs T for $(1/\lambda)$ = 100 cm^{-1}, 200 cm^{-1}, 400 cm^{-1}, 800 cm^{-1} and 1600 cm^{-1}.

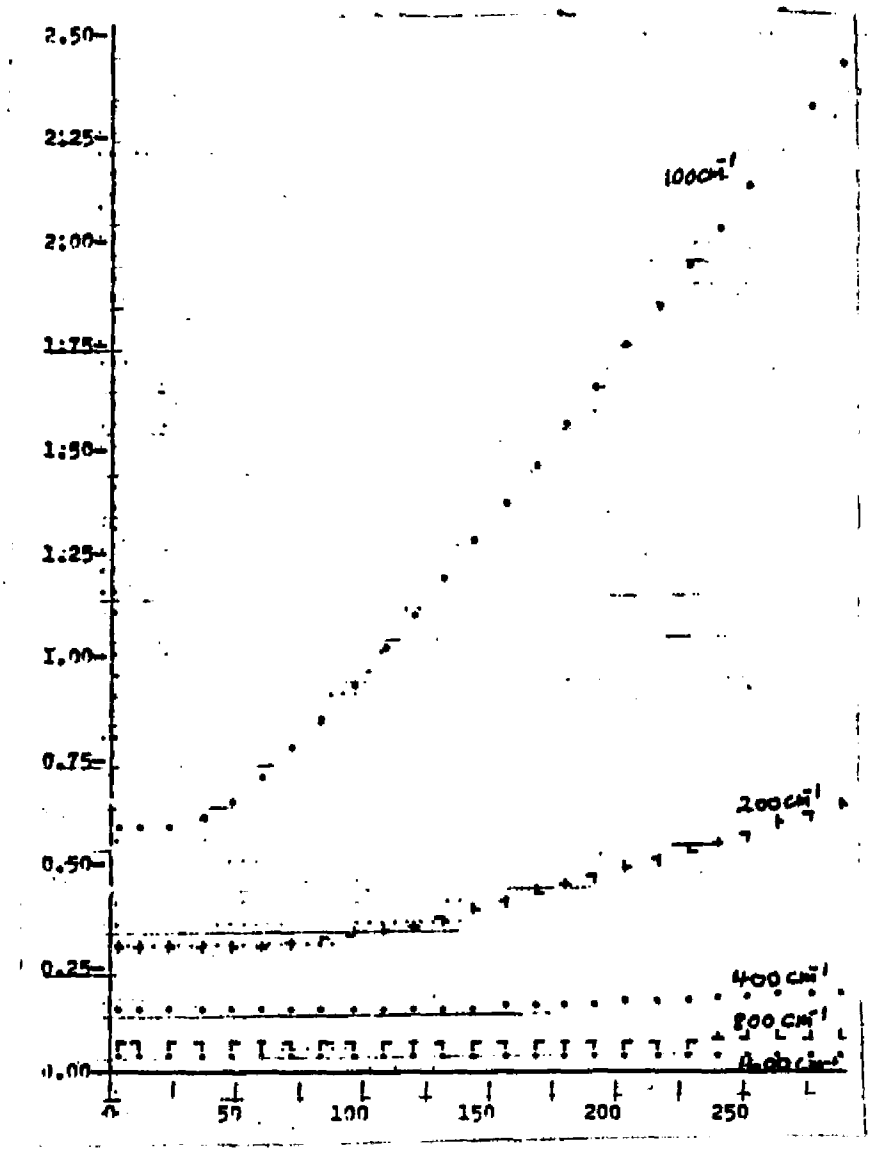

Figure 24 10^{18} $\langle X^2 \rangle$ vs T (°K).

As can be seen, the rms values for $\langle X^2 \rangle$ for values of $1/\lambda$ greater than about 500 cm^{-1} are small enough that they would not be expected to contribute significantly to the value of N in Eq. 21b. As a result, the calculated asymmetry will be small and thus frequencies of $1/\lambda < 500$ cm^{-1} are desirable.

Infrared spectrographic measurements have assigned metal-nitrogen in-plane frequencies ranging from 203 cm^{-1} to 287 cm^{-1} in going from Zn to Ni with a value of 264 cm^{-1} for Co in metalloporphins.[141]

Thus it is certainly reasonable to assume an Fe–N frequency (ω_L) equivalent to $1/\lambda$ in the range 250 cm^{-1} to 300 cm^{-1}. An analysis of the isomer shift data substantiates this assumption.

The value measured for the isomer shift of metallic iron between room temperature and liquid helium temperature is −.118 mm/sec.[160] The differences measured over the same temperature range for the seven complexes (i.e., $\delta_{I293} - \delta_{I4.2}$) are:

Table 11

Isomer shift data for μ-oxo-bis porphyrin complexes (mm/sec)

DIACETYL	−.134
DIPROPIONYL	−.138
PROTO	−.130
MESO	−.141
CYCLOPROPYL	−.144
DEUTERO	−.138

The average value for this quantity is −.138 mm/sec, and the difference between this average and metallic iron can be approximated by the linear temperature dependence of

$$(-.118 - (-.138))/289 = +6.94\times10^{-5} \text{ mm/sec/°K.} \quad (25)$$

The temperature dependence of these isomer shifts arises from two contributing reasons. The chemical shift (due to the physical differences of nuclei surroundings) and a contribution due to the second order Doppler effect which is proportional to the mean square velocity of the Fe^{57} nucleus. The latter contribution can be approximated by:[81]

$$\delta_D = (-9E_R\, k_b/16mc^2)\,[\Theta_d + 8T(T/\Theta_d)^3 \int_0^{\Theta_d/T} x^3\, dx/(e^x-1)]. \quad (26)$$

The approximation of the intrinsic temperature dependence of the isomer shift for these complexes is in close agreement with the value estimated for $FeCl_3$ (also high spin Fe^{3+}) of $(7.0\pm1.5)\times10^{-5}$ mm/sec/°K by Hazony.[81]

An analysis of the second order Doppler effect for that compound reported by Hazony yields a Debye temperature of 400°K. This temperature corresponds to $1/\lambda \approx 275$ cm^{-1}, a reasonable agreement with our approximation. Comparison between these complexes and iron chloride is valid in view of the insignificance of second order crystal field (and covalency) contributions to this effect.

As far as the longitudinal frequency is concerned, we have the infrared determined Fe–O asymmetric stretch frequencies in these compounds of typically about 880 cm^{-1}. This frequency would result in a value of $\langle X_l^2 \rangle$ too small to account for the observed asymmetrical Mossbauer spectrum. However, the Fe–O–Fe symmetric stretch frequency (not observable using infrared spectroscopy) can be approximated to some degree by a normal coordinate analysis of a linear Fe–O–Fe tri-atomic molecule. The ratio of the symmetric frequency (ω_s) to the anti-symmetric frequency (ω_{as}) can be approximated by[83]

$$\omega_s^2 = \omega_a^2 M_{oxygen}/(M_{oxygen} + 2M_{iron}) \qquad (27)$$

This equation sets a value for $(1/\lambda)_{sym}$ at 309 cm^{-1} and for $(1/\lambda)_{anti\text{-}sym}$ at 880 cm^{-1}.

Preliminary Raman spectra of these complexes however yield spectral lines in the range of 100 to 150 cm^{-1} where the symmetric Fe–O–Fe stretch is believed to exist.[175] It is realistic to assume a fraction of the in-plane atoms are coordinated to the iron in its motion transverse to the plane, thus ($\omega_{\parallel}$) should be corrected for by an effective increased mass for the iron, thus decreasing $(1/\lambda)_{sym}$ from its value of 309 cm^{-1}. For example, if the four pyrrole nitrogens were moving with the iron in this mode, M_{iron} could be replaced by $2M_{iron}$ thus predicting $(1/\lambda)_{sym}$ of about 230 cm^{-1}. The observed value is not unreasonable.

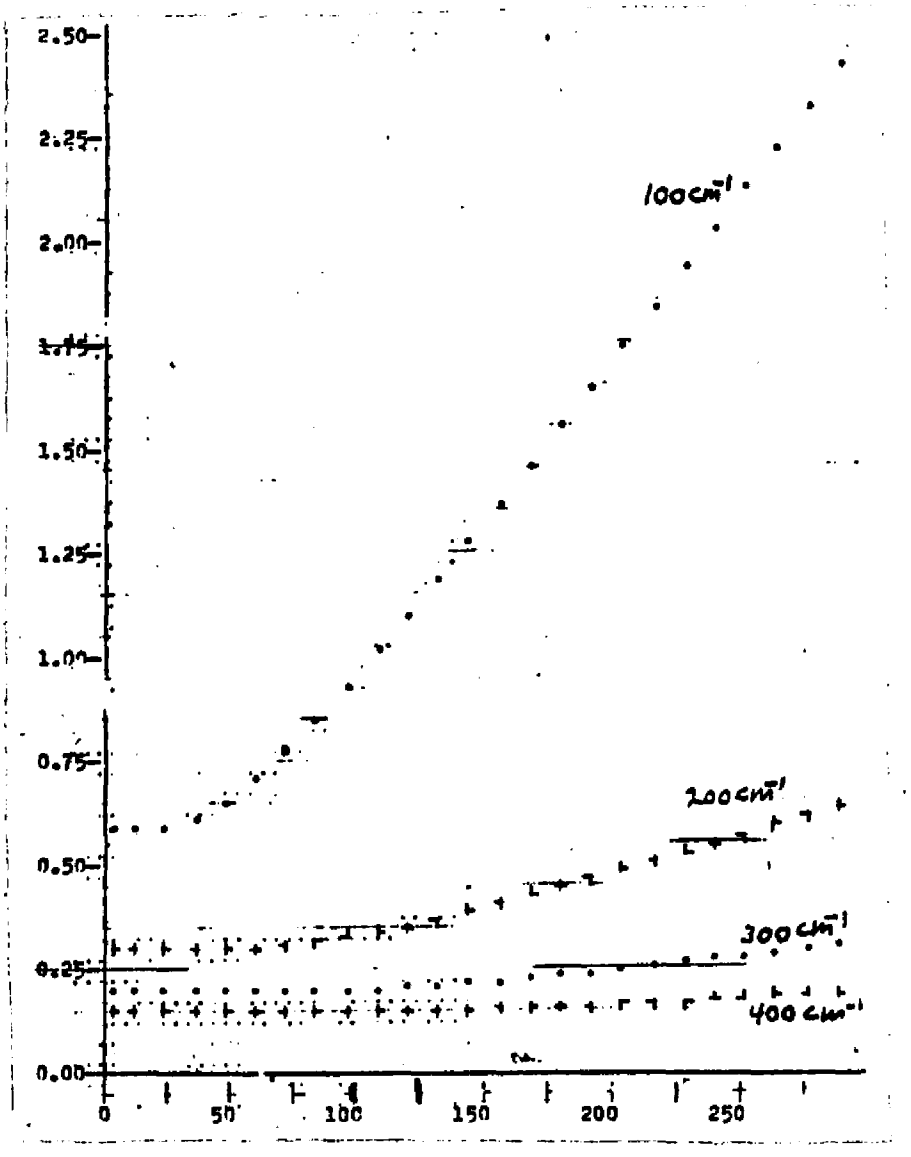

Figure 25 10^{18} $\langle X^2 \rangle$ vs T (°K).

Figure 25 shows a plot of $\langle X^2 \rangle$ vs T for $(1/\lambda) = 100$ cm^{-1}, 200 cm^{-1}, 300 cm^{-1} and 400 cm^{-1}, and Fig. 26 shows six plots of the differences of $\langle X_{\parallel}^2 \rangle_i - \langle X_{\perp}^2 \rangle_j$ vs T, where the i and j subscripts indicate different values for $1/\lambda$.

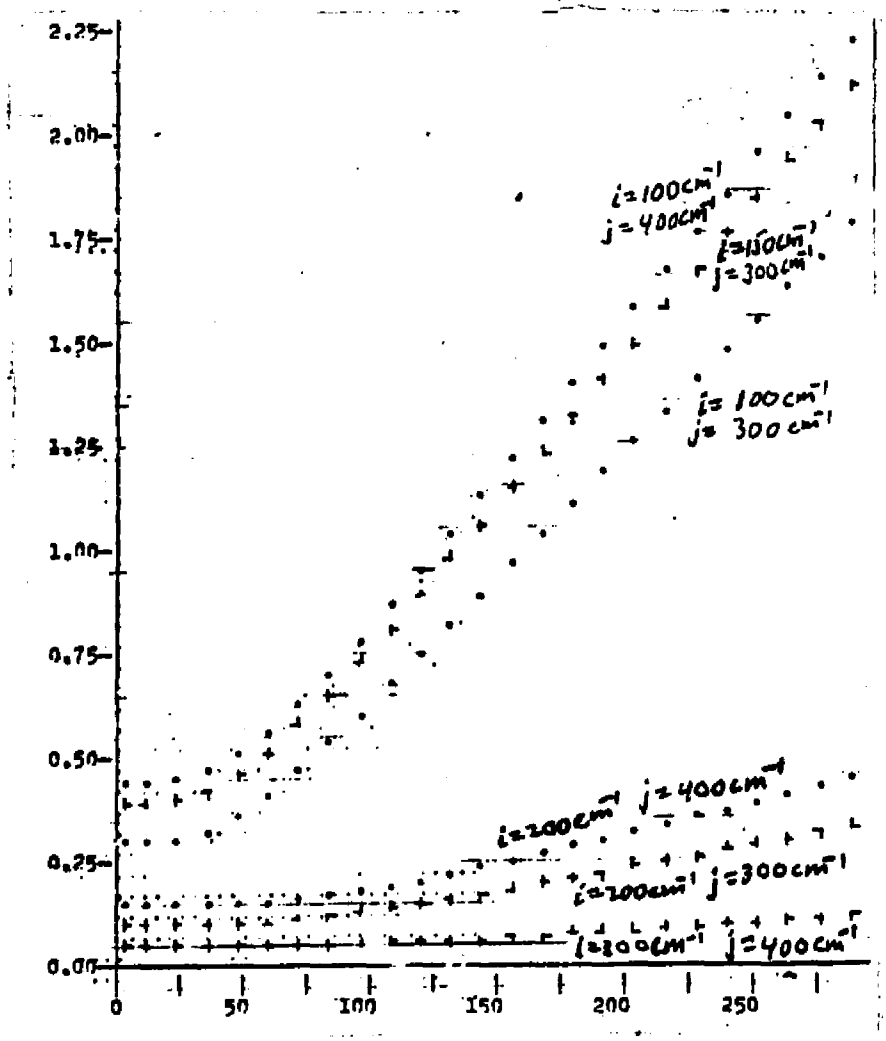

Figure 26 10^{18} ($\langle X_{\parallel}^2 \rangle_i - \langle X_{\perp}^2 \rangle_j$)vs T (°K); i and j refer to values for $1/\lambda$ (cm^{-1}).

The reciprocals of the solutions for Eqs. 21 were then compared to our data using the optical and acoustical temperatures ($\Theta_d = (hc/k_b)(1/\lambda)$) as parameters to determine the best agreement. The results are shown for PROTO, MESO, DIPROPIONYL and DIACETYL in Figs. 27-30 respectively.

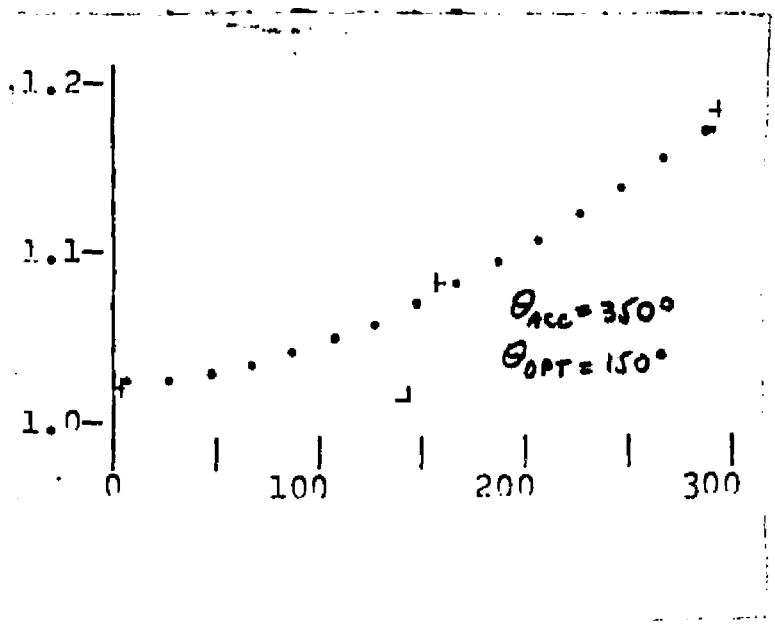

Figure 27 Theoretical Mossbauer asymmetries vs T(°K) with experimentally observed effect for μ-oxo-bis (protohemin dimethyl ester) PROTO.

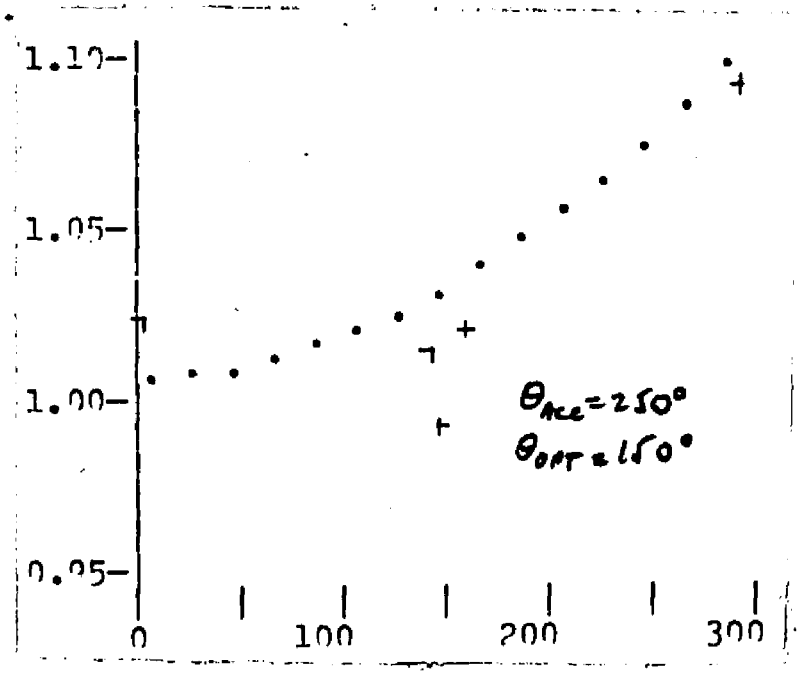

Figure 28 Theoretical Mossbauer asymmetries vs T(°K) with experimentally observed effect for μ-oxo-bis (mesohemin dimethyl ester) MESO.

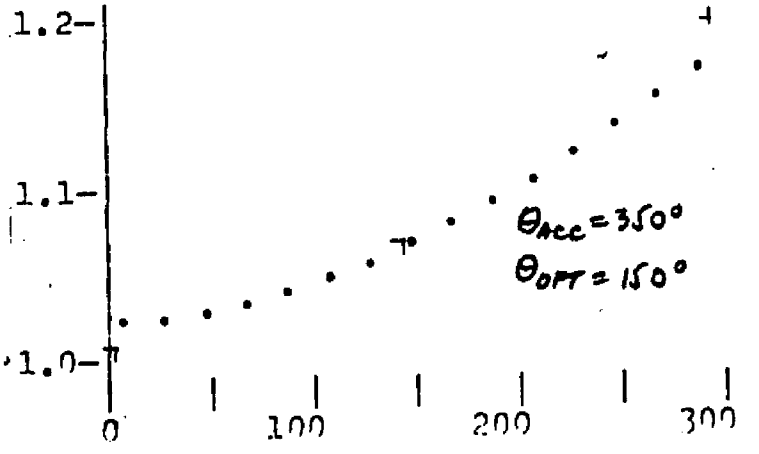

Figure 29 Theoretical Mossbauer asymmetries vs T(°K) with experimentally observed effect for μ-oxo-bis (2,4-dipropionyl deuterohemin dimethyl ester) DIPROPIONYL.

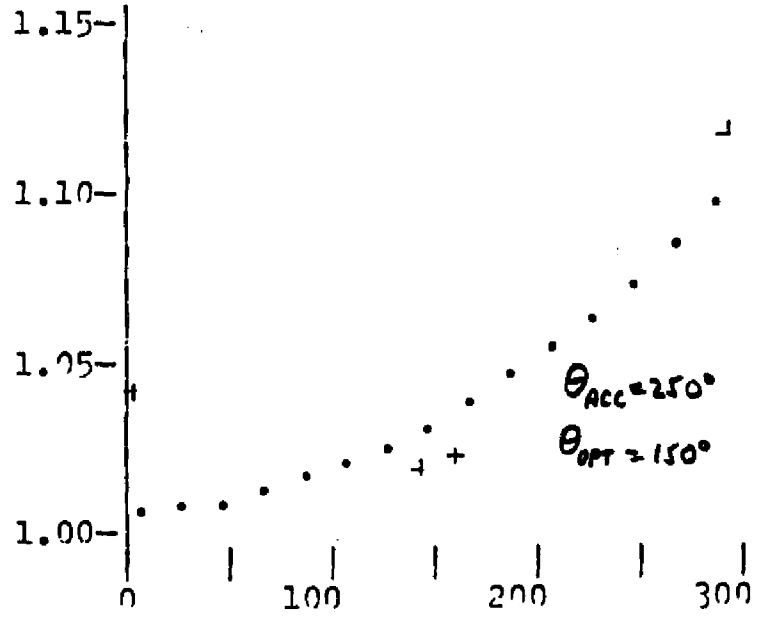

Figure 30 Theoretical Mossbauer asymmetries vs T(°K) with experimentally observed effect for μ-oxo-bis (2,4-diacetyl deuterohemin dimethyl ester) DIACETYL.

It is clear from these figures that there are reasonable frequencies which yield theoretical values for the observed temperature dependent asymmetry observed.

SUMMARY

EXPERIMENTAL APPARATUS AND COMPUTERIZATION

A large amount of time and effort which went into our research was in the design and construction of our high precision Mossbauer apparatus, the hardware interface to a large computer and the interactive program software. Because of the need for transferring large amounts of data to a host computer for later analysis, a unique interface to a large central computer was implemented and extensive software was written to enable ease of control of all the experimental apparatus, data transfer, data analysis and graphical output. This additional large scale investment of time proved to be worthwhile in the simplicity and speed with which data could be transferred from the local storage of the multi-channel analyzer at the experimental site to the host computer. Because of this, the time between termination of one spectral run and the start of another was in many cases only a matter of minutes. Since the experimental apparatus was under computer control, different spectral runs could be started (after data transfer from the run just completed) during non-working hours, thus producing more sets of data than would have been possible without computer control.

It should also be mentioned that because of our investment of time in building the easy-to-use interactive control software, others have been able to use our apparatus efficiently and with a minimum of training.

EXPERIMENTAL PRECISION

The data acquired from our samples using our apparatus in many cases yielded measured standard deviations (determined from many spectral runs) of the order of .001 mm/sec for iron foil calibration spectrum peak separations of 1.677 mm/sec and .002 mm/sec for μ-oxo-bis complexes with peak separations of .545 mm/sec. We feel that this degree of precision in the instrumentation was instrumental in our ability to make the experimental observation of the Gold'anskii Karyagin effect (temperature dependent vibrational anisotropy of atomic motion in the lattice) in an iron complex.

HEMOGLOBIN

By studying hyperfine interactions between the iron nuclear quadrapole moment with the electronic states of the iron ion and contributions of the surrounding environment, we have tried to determine if subtle changes to the hemoglobin molecule structure which are known to affect its function would be reflected at the iron nucleus as determined by Mossbauer spectroscopy. Specifically, using our Mossbauer apparatus, we have determined no significant differences between the hemoglobins of Rhesus monkeys and albino rabbits. This is significant in view of the fact that Rhesus monkey hemoglobin is about 98% a single genetic form and very similar to the hemoglobin of humans while albino rabbit hemoglobin consists of several genetically distinct forms. The results of investigating pH dependencies of the hemoglobin solution using Mossbauer spectroscopy suggested small differences in the quadrapole splitting parameter at 4°K but at 150° to 160°K the statistical accuracy was not sufficient to substantiate the low temperature data. We found a difference in the quadrapole splitting of the Rhesus monkey hemoglobin in whole cells vs that in solution. No difference was observed between the hemoglobin in solution where the DPG had been 'stripped' and the hemoglobin in solution where the DPG had not been 'stripped'. It is possible that DPG which may have been bound to the hemoglobin in the cellular environment (due to possible high levels of DPG in the cell) may have been disassociated from the molecule during dilution and subsequent reconcentration during preparation. A possible cause of the in and out of cell differences observed could be due to binding of DPG to the hemoglobin in the cell.

μ-OXO-BIS PORPHYRIN COMPLEXES

Studies of the μ-oxo-bis antiferromagnetically coupled porphyrin complexes confirmed findings made from other investigative techniques. Specifically, the interpretation of the Mossbauer data confirms that the **Fe-O-Fe** bond angles govern the degree of contribution to the electric field gradient from the crystal field. Also, the electric field gradient nuclear quadrapole moment interactions are consistent with the symmetries indicated by the magnetic coupling constants. Furthermore, reduction of symmetries of the crystal field due to steric hindrances caused by bulky side chains on the porphyrin ring are reflected in the quadrapole splitting parameter.

The most significant finding in our experiments was the observation of the temperature dependent asymmetries of the Mossbauer hyperfine spectrum of the μ-oxo-bis complexes. Analysis of the data confirms that this effect was due to the atomic vibrational anisotropy of iron in the lattice. A theoretical model based on both acoustical (continuous) and optical (discrete) vibrational contributions to the Mossbauer fraction with 'Mossbauer temperatures' in the 250° to 350° range for the continuous modes and 'Mossbauer temperatures' of 150° for the discrete modes yields good agreement with our data. The low optical frequency is believed to be characteristic of the symmetric stretch frequency of the iron-oxygen-iron bond between the two porphyrin complexes.

SUGGESTIONS FOR FUTURE STUDY

Based on our findings an experiment should be done to determine if DPG binding to hemoglobin was the cause of the in and out of cell differences observed in our Mossbauer experiments. Specifically, hemoglobin in solution which has been 'stripped' of DPG should be compared with a similar preparation to which DPG has been re-bound. Additional Mossbauer study of the μ-oxo-bis porphyrin complexes is also warranted given the temperature dependent asymmetries we observed. The presence of large external magnetic fields would further split the spectral lines and thus yield additional information about the iron environment.

APPENDIX I

EXPERIMENTAL COMPUTER PROGRAMMING COMMANDS AND DISCUSSION

Before discussing the command structure of the programming, some basic concepts of the VM/370 CMS system should be understood.

CMS is the Conversational Monitor System which runs the user's virtual computer under the basic control programming (CP) of VM/370. A disk file is a CMS formatted data set on a direct access storage device (magnetic disk) specified by a file name and a file type. The user may read from his disk (into main storage of the computer) the contents of any disk file or write (from main storage) to his disk the contents of any disk file. If a disk file is read into storage and its contents changed, the permanent copy on disk is not changed unless explicitly overwritten by a changed version.

A CMS EXEC procedure is a special type of disk file which, when read into a specific region of main storage, will cause the user's virtual computer to execute a series of commands as specified in the file. When the user causes an EXEC procedure to be executed, parameters may be passed to the routine. In order to begin execution of our interactive program, an EXEC procedure was invoked, which dynamically assigned data set reference numbers to disk files whose names were entered as part of a parameter list. For example, the CMS command XEQ DMAIN *fname1 ftype1* (*fname2 ftype2*) would cause the exec procedure XEQ to be executed as follows:

Disk file *fname1 ftype1* would be assigned one data set reference number and optionally the disk file *fname2 ftype2* would be assigned another data set reference number. (A brief note on convention: (a) means a is an optional parameter while <a|b> means you must choose between a and b.)

After setting up special virtual machine configurations, the procedure caused DMAIN, the name of our interactive control program, to be loaded into main storage for execution. From this point on until termination of the program, the disk files *fname1 ftype1* and (*fname2 ftype2*) are referred to as INPUT and (OUTPUT) files respectively within the command structure in our program.

The program begins by typing a prompting character ('=') at the terminal after which it waits for the user to type in a command. After the completion of each command, the user is always prompted to enter a new command.

LIST OF MOST USED COMMANDS IN PROGRAM DMAIN

READ <INPUT | OUTPUT | SCRATCH | 'FILENAME FILETYPE'>

Reads into main storage the contents of the specified file. (The 'scratch file' is used to store on disk interim calculational results).

DUMP (QUARTER | HALF | ALL)

Directs the Research Device Coupler to communicate with the multi-channel analyzer so as to transfer the stored information into the corresponding elements of data array in main storage. The options will cause 256, 512 or 1024 channels of MCA memory to be dumped. The default is 1024 channels. The input disk-file is immediately updated upon completion of a dump.

INPUT (n a b...r | 'LITERAL EXPRESSION')

This command will store the values a,b,...r in the data array (1023) elements sequentially beginning at element n. If an expression of up to 120 characters is entered between quotes, it is stored as a label for the contents of file information in memory.

LABEL

Causes the current label of the file to be typed at the terminal.

EDIT

Allows the user to edit any portion of the current label without having to re-type the entire line. It is self documented within the program by typing a ? while in this mode.

TYPE (n m)

Causes the current values of the data to be typed at the terminal from element n to element m.

WRITE (INPUT | OUTPUT | SCRATCH)

Updates the contents of the appropriate disk-file with the contents of main storage.

CLEAR

Sets all data elements to a value of zero.

SMOOTH

Invokes a running smoothing of the data locally by a third degree least squares fit.

ADD (number)

Adds the value of number to all the elements of the data array.

PARA

Lists the current values of 6 parameters, XX, YY, ZZ, UU, VV, WW.

SET XX = a,... WW = g

Allows the user to set any combination of parameters to new values.

COMPUTE

Stores the value of the parameter UU for the values of the data between elements determined by the values of the parameters VV and WW.

BADPOINT

Compares each data point to two neighboring points on either side. If the value is greater than 20 standard deviations of the four neighbors, its value is set to the average of the four points.

NBASE

Determines the average value of the data between elements determined by the values of XX and YY.

GETPEAK (n)

Causes a least squares fit of n Lorentzians to the data. It stores in memory the calculated values based on the fit and also the locations of each peak, their half-widths at half maximum and adjusted amplitudes (intensity/background).

TGET

Types information stored as a result of Lorentzian fit of GETPEAK.

LIST

Lists all parameters (user-chosen code *classifications*) which will be used in converting peak locations and line widths in the energies. A *classification* refers to a 1 to 4 digit code which can be referred to the particular MCA settings used for the spectral accumulation.

FIT

Instructs the user to enter parameters for a new *classification* or change any existing ones.

SAVE

Writes on a special parameter disk-file all existing conversion parameters. The contents of this file are loaded in the main storage at the beginning of the program.

VELO (code *classification*)

Converts computed peak locations and half widths into energies as determined by the appropriate parameters listed by the LIST command.

USEP

Types out the separations of the peaks in energies.

SEP

Types out the separations of the peaks in channel numbers.

ISO (n m)

Types out the displacement (in energy) of the center of gravity of the number peaks n and m from some standard location (isomer shift). This location is the center of gravity of a standard spectrum.

ANGLE (code *classification*)

Adjusts the values of the data according to a parameter in the appropriate *classification*.

SOLID

Determines the value of the parameter used by the ANGLE command. This command is used when the data represents a solid angle calibration spectrum.

SIMULATE

Branches to a routine which will prompt the user to enter peak locations, half widths and intensities of Lorentzian curves. A theoretical function will then generate values for the data based on a sum of these Lorentzian lines.

PRINT

Causes a printout of the vital parameters and the data on a remote printer.

PLOT

Branches to a special plotting mode in which there is a subset of commands. All I/O from this mode is directed to the Research Device Coupler which in turn will drive a Tektronix 611 storage scope whose resolution (in raster units) is 1024 by 1024.

SCOPE (a, b, c, d)

Maps the scope coordinates into a size determined by the left margin, right margin, bottom margin and top margins; a, b, c and d (in raster units).

For example, if a=100, b=50, c=200 and d=500 the full window available for plotting will be defined (in raster units) by the boundaries lower left = (99, 199), lower right = (973, 199), upper left = (99, 723) and upper right = (973, 923). The scope parameters remain in effect until explicitly changed or upon each re-entry to the plotting mode. The default values for a, b, c and d are 10, 10, 120 and 10 respectively.

SCALE <a, b>

Scales the data x(i) vs i to the currently defined window (by the scope command). The options a and b define the starting and ending elements of the data to be scaled. The default values for a and b are 1 and 1000 respectively.

PLOT (LINE | POINT) <a, b,> <expand>

Plots the data on the scope as determined by their scaled values. The (point | line) option will cause discrete points or connected lines to be drawn. The first and last elements of the data points to be plotted are determined from the last values set by the SCALE command (or their defaults) or the new values of a and b if entered. The expand option is equivalent to rescaling to the new values of a and b entered.

ERASE

Erases the storage scope.

RETURN

Returns from the plotting mode to the main program.

PLAB

Writes on the scope (in the region $0 \leq y \leq 120$) the current label for the file in main storage. This command is in the main program.

FILE

Issues a request for the file name of the file currently in main storage, the name of the sample used in the spectrum acquisition and the temperature at which the spectrum was accumulated. A special CMS disk file is then updated with the latest record containing the calculated parameters for the current data file in main storage. These parameter values (including the isomer shift, temperature and % effect) form a separate entry in this special file. By using sort facilities available in CMS, information can be sorted with respect to any parameter as well as serving as a permanent record of the contents of any data file.

§STOP

Terminates the program

By using the CMS functions, old data files can be put on tape for permanent storage (and re-read onto disk if necessary). The FILE (command) serves as an index of all data files as well as a data base for comparative analysis.

One other command in the main program not described is the calculator mode request, §CALCULATOR (ON/OFF). By entering the calculator mode, instant interpretation and evaluation of most FORTRAN IV assignment statements is available so that arbitrary calculations may be made without ever having to interrupt execution of the main program.

REFERENCES

1. Alben, J. O., Fuchsman, W. H., Beaudreau, C. A. and Caughey, W. S., 1968, *Biochemistry*, 7, No. 2, 624-635.

2. Alekseevskii, N. E., Hien, P. Z., Shapiro, V. G. and Shpinel, V. S., 1963, *Soviet Physics JETP* **16**, No. 3, 559-561.

3. Alekseevskii, N. E., Kir'yanov, A. R., Nizhankovskii, V. I. and Samarskii, Y. A., 1965, *Institute of Physics Problems, U.S.S.R. Academy of Sciences*, 171-177.

4. Alpert, Y., Banerjee, R. and Denis, J., 1973, *Nature New Biology* **243**, 80-81.

5. Alpert, B. and Banerjee, R., 1972, *Biochemical and Biophysical Research Communications* **46**, No. 2, 913-919.

6. Alpert, B., Banerjee, R. and Lindqvist, L., 1974, *Proc. National Academy of Sciences U.S.A.* **71**, No. 2, 558-562.

7. Alpert, B. and Banerjee, R., 1972, *Biochemical and Biophysical Research Communications* **46**, No. 2, 913-919.

8. Antonini, E., Anderson, N. M. and Brunori, M., 1972, *Journal of Biological Chemistry* **247**, No. 1, 319-321.

9. Antonini, E. and Brunori, M., 1970, *Annual Review of Biochemistry* **39**, 977-1041.

10. Antonini, E. and Brunori, M., 'Hemoglobin and Myoglobin in their Reactions with Ligands' *Frontiers of Biology* Vol. 21 (1971), North-Holland Publishing Co., Amsterdam.

11. Arone, A. and Perutz, M. F., 1974, *Nature* **249**, 34-36.

12. Austin, R. H., Beeson, K. W., Frauenfelder, H. and Gunsalus, I. C., 'Dynamics of Ligand Binding to Myoglobin' submitted to *Biochemistry* August 1974.

13. Austin, R. H., Beeson, K., Eisenstein, L., Frauenfelder, H., Gunsalus, I. C. and Marshall, V. P., 1974, *Physical Review Letters* **32**, No. 8, 403-405.

14. Austin, R. H., Beeson, K., Eisenstein, L., Frauenfelder, H., Gunsalus, I. C. and Marshall, V. P., 1973, *Science* **181**, 541-543.

15. Barlow, C. H., Maxwell, J. C., Wallace, W. J., and Caughey, W. S., 1973, *Biochemical and Biophysical Research Communications* **55**, No. 1.

16. Baucroft, G. M. and Libbey, E. T., 1973, *Journal Chemical Society Dalton*, 2103-2110.

17. Bausil, R. Herzfeld, J. and Stanley, H. E., 1974, *Science* **186**, 929-932.

18. Benesch, R. E., Benesch, R., Renthal, R. D. and Maeda, N., 1972, *Biochemistry* **11**, No. 19, 3576-3582.

19. Benesch, R., Benesch, R. E. and Yu, C. I., 1968, *Proc. National Academy of Sciences U.S.A.* **59**, 256.

20. Benesch, R. E., Benesch, R. and Yu, C. I., 1969, *Biochemistry* **8**, 2567.

21. Benesch, R., Benesch, R. E. and Enski, Y., 1968, *Proc. National Academy of Sciences U.S.A.* **61**, 1102.

22. Benesch, R. and Benesch, R. E., 1967, *Biochemical and Biophysical Research Communications* **26**, 162.

23. Bleaney, B. and Stevens, K. W. H., 'Paramagnetic Resonance' in *Progress in Physics* Vol. 16 (1953), 108-159.

24. Blume, M., 1965, *Physical Review Letters* **14**, No. 4, 96-98.

25. Bonaventura, J. and Riggs, A., 1967, *Science* **158**, No. 3802, 800-802.

26. Bonaventura, J., 1969, *Biochemical Genetics* **3**, No. 239, 239-247.

27. Bonaventura, C., Bonaventura, J., Antonini, E. and Brunori, M., 1973, *Biochemistry* **12**, No. 18, 3424-3428.

28. Borsook, H., Teigler, D. and Gunderson, A., 1968, *Archives of Biochemistry and Biophysics* **125**, 429-435.

29. Boyd, P. D. W. and Smith, T. D., 1971, *Inorganic Chemistry* **10**, No. 9, 2041-2043.

30. Brenna, M., Luzzana, M., Pace, M., Perrella, M., Rossi, R., Rossi-Bernardi, L. and Roughton, F. J. W., 1972, *Advances in Experimental Medicine and Biology* **28**, 19-40.

31. Brill, A. S., 1972, *Molecular Physics* **24**, No. 4, 787-800.

32. Brunori, M., Bonaventura, J., Bonaventura, C., Antonini, E. and Wyman, J., 1972, *Proc. National Academy of Sciences U.S.A.* **69**, No. 4, 868-871.

33. Brunori, M. and Schuster, T. M., 1969, *Journal of Biological Chemistry* **244**, No. 15, 4046-4053.

34. Bulen, W. A., LeComte, J. R. and Lough, S., 1973, *Biochemical and Biophysical Research Communications* **54**, No. 4, 1274-1281.

35. Bull, T. E., andrasko, J., Chiancone, E. and Forsen, S., 1973, *Journal of Molecular Biology* **73**, 251-259.

36. Caldwell, P. R. B., Nagel, R. L. and Jaffe, E. R., 1971, *Biochemical and Biophysical Research Communications* **44**, No. 6, 1504-1509.

37. Campbell, I. D., Dobson, C. M., Williams, R. J. P. and Xavier, A. V., 1973, *Journal of Magnetic Resonance* **11**, 172-181.

38. Caughey, W. S., Fujimoto, W. Y. and Johnson, B. P., 1966, *Biochemistry* **5**, 3830.

39. Caughey, W., Smythe, G. A., McDaniel, M. C. and Barlow, C. H., 1975, 'Magnetic Resonance and Electronic Spectra of μ-oxo-bis (protohemin) and Protoheme', unpublished.

40. Chang, C. K. and Traylor, T. G., 1973, *Journal of the American Chemical Society* **95**, 8475-8477.

41. Chang, C. K. and Traylor, T. G., 1973, *Journal of the American Chemical Society* **95**, 8477-8479.

42. Chang, C. K. and Traylor, T. G., 1973, *Journal of the American Chemical Society* **95**, 5810-5811.

43. Chang, C. K. and Traylor, T. C., 1973, *Proc. National Academy of Sciences U.S.A.* **70**, No. 9, 2647-2650.

44. Chanutin, A. and Curnish, R. R., 1967, *Arch. Biochemical Biophysical Research Communications* **121**, 96.

45. Cohen, I. A., 1969, *Journal of the American Chemical Society* **91**, No. 8, 1980-1983.

46. Cohen, S. G., Gielen, P. and Kaplow, R., 1966, *Physical Review* **141**, No. 1, 423-424.

47. Collman, J. P., Gagne, R. R., Reed, C. A., Robinson, W. T. and Rodley, G. A., 1974, *Proc. National Academy of Sciences U.S.A.* **71**, No. 4, 1326-1329.

48. Collman, J. P., Gagne, R. R., Gray, H. B. and Hare, J. W., 1974, *Journal of the American Chemical Society* **96**, No. 20, 6522-6524.

49. Collins, R. L. and Travis, J. C., 'The Electric Field Gradient Tensor' in *Mossbauer Effect Methodology* Vol. 3 (1967), Plenum Press, New York.

50. Cranshaw, T. E., 1973, *Journal of Physics E: Scientific Instruments* **6** (Great Britain), 1053-1057.

51. Damus, P. S., Hicks, M. and Rosenberg, R. D., 1973, *Nature* **246**, 355-357.

52. Dayhoff, M. O., *Atlas of Protein Sequence and Structure* **4** (1969), National Biomedical Research Foundation, Silver Spring, Maryland.

53. Debrunner, P., Tsibris, J. C. M. and Münck, E., Eds., *Mossbauer Spectroscopy in Biological Systems Proceedings* (1969), University of Illinois Bulletin, Urbana, Illinois.

54. Delyagin, N. N., Mitrofanov, K. P. and Nesterov, V. I., 1972, *Nuclear Instruments and Methods* **100**, 315-316.

55. Dickerson, R. E., 1972, *Annual Review of Biochemistry* **41**, 815-842.

56. Dickerson, R. E. and Geis, I., *The STructure and Action of Proteins* (1969), Harper and Row, New York.

57. Eaton, J. W., Skelton, T. D. and Berger, E., 1974, *Science* **183**, 743-744.

58. Epstein, L. M. and Straub, D. K., 1969, *Inorganic Chemistry* **8**, No. 3, 560-562.

59. Falk, J. E., *Porphyrins and Metalloporphyrins* B. B. A. Library Vol. 2 (1964), Elsevier Publishing Co., Amsterdam.

60. Farwell, K. J. and McMeekin, T. L., 1973, *Archives of Biochemistry and Biophysics* **158**, 702-710.

61. Fleischer, E. B. and Srivastava, T. S., 1963, *Journal of the American Chemical Society* **91**, No. 9, 2403-2405.

62. Fleischman, M. 'In Vitro Measurements of Uncombined Oxygen Concentration in Intact Red Cells' in *Blood Oxygenation* (1970), Plenum Press, New York, 107-115.

63. Frauenfelder, H., *The Mossbauer Effect* (1962), W. A. Benjamin, New York.

64. Fuchsman, W. H., Barlow, C. H., Wallace, W. J. and Caughey, W. S., 1975, 'Novel Heme: O_2 Bonding of Possible Relevance to Oxygen Utilizing Heme and Other Proteins', pre-press communication.

65. Garby, L., Gerber, G. and DeVerdier, C. M., 1969, *European Journal of Biochemistry* **10**, 110.

66. Gibb, T. C., Greatrex, R. and Greenwood, N. N., 1968, *Journal Chemical Society* (A), 890-894.

67. Gibb, T. C., Greatrex, R., Greenwood, N. N. and Thompson, D. D., 1967, *Journal Chemical Society* (A), 1663.

68. Gibson, Q. H., 1970, *Biochemical and Biophysical Research Communications* **40**, No. 6, 1319-1324.

69. Gill, D., Salmeen, I. T. and Rimai, L., 1973, *Journal of Biological Chemistry* **248**, No. 14, 5211-5213.

70. Gilen, R. G. and Riggs, A., 1973, *Journal of Biological Chemistry* **248**, No. 6, 1961-1969.

71. Gold'anskii, V. I. and Herber, R. H., Eds., *Chemical Applications of Mossbauer Spectroscopy* (1968), Academic Press, New York.

72. Gold'anskii, V. I., *The Mossbauer Effect and Its Applications in Chemistry* (1964) Consultants Bureau, New York.

73. Gonser, U., 1962, *Journal of Physical Chemistry* **66**, 564.

74. Goodenough, J. B., *Magnetism and the Chemical Bond* (1963), Interscience, New York.

75. Gould, R. F., Ed., *The Mossbauer Effect and its Application in Chemistry*, Advances in Chemistry Series 68 (1967), American Chemical Society, Washington, D. C.

76. Gray, R. D. and Gibson, Q. H., 1971, *Journal of Biological Chemistry* **246**, No. 16, 5176-5178.

77. Gray, R. D. and Gibson, Q. H., 1971, *Journal of Biological Chemistry* **246**, No. 23, 7168-7174.

78. Greenwood, T. C. and Gibb, N. N., *Mossbauer Spectroscopy* (1971), Chapman and Hall Ltd., London.

79. Harkness, D. R., Roth, S., Goldman, P. and Goldberg, M., 1972, *Advances in Experimental Medicine and Biology* **28**, 415-430.

80. Harris, G., 1968, *Journal of Chemical Physics* **48**, No. 5, 2191-2214.

81. Hazony, Y., 1973, *Physical Review B* **7**, No. 7, 3309-3314.

82. Henry, Y. and Banerjee, R., 1973, *Journal of Molecular Biology* **73**, 469-482.

83. Herzberg, G., *Molecular Spectra and Molecular Structure II. Infrared and Raman Spectra of Polyatomic Molecules*, D. Van Nostrand Company, Inc., New York.

84. Herber, R. H. and Chandra, S., 1970, *Journal of Chemical Physics* **52**, No. 12, 6045-6048.

85. Herzfeld, J. and Stanley, H. E., 1972, *Biochemical and Biophysical Research Communications* **48**, No. 2, 307-313.

86. Hill, H. A. O. and Morallee, K. G., 1972, *Journal of the American Chemical Society* **94**, No. 3, 731-738.

87. Ho, C. and Lindstrom, T. R., 1972, *Advances in Experimental Medicine and Biology* **28**, 65-76.

88. Holland, R. A. B., 'Factors Determining the Velocity of Gas Uptake by Intracellular Hemoglobin' in *Blood Oxygenation* (1970), Plenum Press, New York, 1-23.

89. Horroceks, W. D. Jr. and Greenberg, E. S., 1973, *Biochimica et Biophysica Acta* **322**, 38-44.

90. Huisman, T. H. J. and Schroeder, W. A., *New Aspects of the Structure, Function and Synthesis of Hemoglobins* (1971), CRC Press, Cleveland, Ohio.

91. Huynh, B. H., Papaefthymiou, G. C., Yen, C. S., Groves, J. L. and Wu, C. S., 'Electronic Structure of Fe^{2+} in Normal Human Hemoglobin and Its Isolated Subunits' (1974), Department of Physics, Columbia University, New York, pre-publication.

92. Iizuka, T. and Yonetani, T., 1970, *Advances in Biophysics* **1**, 157-182.

93. Imamura, T. and Riggs, A., 1972, *Biochemical Genetics* **7**, 127-130.

94. Jahn, H. A. and Teller, E., 1937, *Proceedings of the Royal Society A* **161**, 220.

95. Johnson, C. E., 1971, *Journal of Applied Physics* **42**, No. 4, 1325-1331.

96. König, E., Riter, G. and Kanellakopulos, B., 1973, *Journal of Chemical Physics* **58**, No. 7, 3001-3009.

97. Kagan, Y. and Maslov, V. A., 1962, *Soviet Physics JETP* **14**, No. 14, 922-927.

98. Kagan, Y., 1962, *Soviet Physics DOKLADY* **6**, No. 10, 881-882.

99. Kagan, Y., 1965, *Soviet Physics JETP* **20**, No. 1, 243-250.

100. Kanzmann, W., *Quantum Chemistry* (1957), Academic Press, New York.

101. Kilmartin, J. V., 1973, *Biochemical Journal*, **133**, 725-733.

102. Kotani, M., 1960, *Supplement of the Progress of Theoretical Physics*, No. 14, 1-16.

103. Kotani, M. *Advances in Quantum Chemistry* Vol. 4 (1968), ed. P. O. Lowdin, Academic Press, New York, 227.

104. Kramers, H. A., *Quantum Mechanics* (1957), North-Holland Publishing Co., Amsterdam.

105. Krasney, S. and Graczyk, J. F., 1975, 'Scanning Electron Diffractometry Utilizing a Research Device Coupler', IBM Research Report RC5300.

106. Krasney, S. and Lilienthal, H., 1975, 'Faraday Magnetic Susceptometry Utilizing a Research Device Coupler', IBM Research Report RC5504.

107. Kubo, R. and Nagamiya, T., Eds., *Solid State Physics* (1968), McGraw-Hill Book Co. Inc., New York.

108. Lambeth, D. O. and Palmer, G., 1973, *Journal of Biological Chemistry* **248**, No. 17, 6095-6103.

109. Lane, R. S., 1973, *Biochimica et Biophysica Acta* **320**, 133-142.

110. Lang, G., 1970, *Quarterly Review of Biophysics* 3, No. 1, 1-60.

111. Lang, G., 'Application of the Mossbauer Effect in Biology', *United Kingdom Atomic Energy Authority Research Group Report*, (1969) Atomic Energy Research Establishment, Harwell, Berkshire.

112. Lang, G. and Marshall, W., 1966, *Proc. Physics Society* 87, 3-34.

113. Lang, G. and Oosterhuis, W. T., 'Calculated Paramagnetic Mossbauer Spectra of Spin 1/2 Iron Salts' *United Kingdom Atomic Energy Authority Research Group Report* (1969), Atomic Energy Research Establishment, Harwell, Berkshire.

114. Lewis, J., Mabbs, F. E. and Richards, A., 1967, *Journal Chemical Society (A)*, 1014-1018.

115. Lian, C. Y., Roth, S. and Harkness, D. R., 1971, *Biochemical and Biophysical Research Communications* **45**, No. 1, 151-158.

116. Lindstrom, T. R., Baldassare, J. J., Burn, H. F. and Ho, C., 1973, *Biochemistry* **12**, No. 21, 4212-4217.

117. Lippard, S. J., Schugar, H. and Walling, C., 1967, *Inorganic Chemistry* **6**, No. 10, 1825-1831.

118. MacQuarrie, R. and Gibson, Q. H., 1972, *Journal of Biological Chemistry* **247**, No. 18, 5686-5694.

119. MacQuarrie, R. and Gibson, Q. H., 1971, *Journal of Biological Chemistry*, **246**, No. 18, 5832-5836.

120. Maeda, T., Imai, K. and Tyuma, I., 1972, *Biochemistry* **11**, No. 20, 3685-3689.

121. Maricondi, C., Straub, D. K. and Epstein, L. M., 1972, *Journal of the American Chemical Society* **94**, No. 12, 4157-4159.

122. Maricondi, C. Swift, W. and Straub, D. K., 1969, *Journal of the American Chemical Society* **91**, No. 19, 5205-5210.

123. Matwiyoff, N. A., Vergamini, P. J., Needham, T. E., Gregg, C. T., Volpe. J. A. and Caughey, W. S., 1973, *Journal of the American Chemical Society* **95**, No. 13, 4429-4430.

124. Mayer, A., Ogawa, S. and Shulman, R. G., 1973, *Journal of Molecular Biology* **81**, 187-197.

125. McConnell, H. M., 1971, *Annual Review of Biochemistry* **40**, 227-236.

126. McCray, J. A., 1972, *Biochemical and Biophysical Research Communications* **47**, No. 1, 187-193.

127. Melissinos, A. C., *Experiments in Modern Physics* (1971), Academic Press, New York.

128. Merrithew, P. B. and Rasmussen, P. G., 1972, *Inorganic Chemistry* **11**, No. 2, 325-330.

129. Monod, J., Wyman, J. and Changeux, J. P., 1965, *Journal of Molecular Biology* **12**, 88.

130. Morris, A. J. and Liang, K., 1968, *Archives of Biochemistry and Biophysics* **125**, 468-479.

131. Moss, T. H., Lilienthal, H. R. and Moleski, C., 1972, *Journal Chemical Society: Chem. Comm.*, 263-264.

132. Moss, T. H., Bearden, A. J. and Caughey, W. S., 1969, *Journal of Chemical Physics* **51**, No. 6, 2624-2631.

133. Moss, T. H., 1974, 'Applications of Physics in Biology', unpublished.

134. Moss, T. H., 'Mossbauer Spectroscopy of Iron Proteins', invited paper, New York Meeting of the American Physical Society, February, 1969.

135. Muirhead, H., Cox, J. M., Mazzarella, L. and Perutz, M. F., 1967, *Journal Molecular Biology* **28**, 117-156.

136. Nakano, N., Otsuka, J. and Tasaki, A. *IEEE Transactions on Magnetics* Sept. 1972, 413-415.

137. Nakamura, T., Sugita, Y. and Bannai, S., 1973, *Journal of Biological Chemistry* **248**, No. 14, 1119-1122.

138. Nelson, S. M., Bryan, P. and Busch, D. H., 1966, *Chemical Communications* No. 18, 641-642.

139. Noren, I. B. E., Ho, C. and Casassa, E. F., 1971, *Biochemistry* **10**, No. 17, 3222-3229.

140. O'Keefe, D. H., Barlow, C. H., Smythe, G. A., Fuchsman, W. H., Moss, T. H., Lilenthal, H. R. and Caughey, W. S., 1975, 'Magnetic and Spectroscopic Probes for Fe-O-Fe Linkages in Hemin Systems', *BioInorganic Chemistry*, in press.

141. Ogoshi, H., Saito, Y. and Nakamoto, K., 1972, *Journal of Chemical Physics* **57**, No. 10, 4194.

142. Olson, J. S. and Gibson, Q. H., 1970, *Biochemical and Biophysical Research Communications* **41**, No. 2, 421-426.

143. Olson, J. S., andersen, M. E. and Gibson, Q. H., 1971, *Journal of Biological Chemistry* **246**, No. 19, 5919-5923.

144. Oosterhuis, W. T., 'Paramagnetic Hyperfine Structure in Iron Complexes with Effective Spin S=1/2' in *Mossbauer Effect Methodology* Vol. 7 (1971), Plenum Press, New York, 97-121.

145. Oosterhuis, W. T., Weaver, D. L. and Paez, E. A., 1974, *Journal of Chemical Physics* **60**, No. 3, 1018-1025.

146. Oosterhuis, W. T. and Vicaro, P. J., 1972, *Biochimica et Biophysica Acta* **264**, 11-16.

147. Oosterhuis, W. T. and Lang, G., 1969, *Journal of Chemical Physics* **50**, No. 10, 4381-4387.

148. Otsuka, J., Matsuoka, O., Fuchikami, N. and Seno, Y., 1973, *Journal of the Physical Society of Japan* **35**, No. 3.

149. Parak, V. F. and Formanek, H., 1971, *Acta Cryst.* A27, 573.

150. Parkhurst, L. J. and Gibson, Q. H., 1967, *Journal of Biological Chemistry* **242**, No. 24, 5762-5770.

151. Pasternak, M. and Sonnino, T., 1968, *Journal of Chemical Physics* **48**, No. 5, 2004-2009.

152. Pasternak, M., Simopoulous, A. and Hazony, Y., 1965, *Physical Review* **140**, No. 6A, 1892-1896.

153. Perkins, H. K. and Hazony, Y., 1972, *Physical Review B* **5**, No. 1, 7-18.

154. Perutz, M. F., Muirhead, H., Cox, J. M. and Goamen, L. C. G., 1968, *Nature* **219**, 131.

155. Perutz, M. F., 1970, *Nature* **228**, 726.

156. Perutz, M. F., 1973, *Biochem. Society Transactions* **1**, 42.

157. Pfeiffer, L. and Lichtenwainer, C. P., 1973, *Review Scientific Instrumentation* **44**, No. 10, 1500-1501.

158. Philips, J. N., 1960, *Review of Pure Applied Chemistry* **10**.

159. Phillipson, P. E., Ackerson, B. J. and Wyman, J., 1973, *Proc. National Academy of Sciences U.S.A.* **70**, No. 5, 1550-1553.

160. Preston, R. S., Hanna, S. S. and Herberle, J., 1962, *Physical Review* **128**, No. 5, 2207-2218.

161. Pulsinelli, P. D., Perutz, M. F. and Nagel, R. L., 1973, *Proc. National Academy of Sciences U.S.A.* **70**, No. 12, Part II, 3870-3874.

162. Reed, T., Bunkenberg, J. and Chance, B. 'Laser Photolysis of Crystalline Carbonmonoxyhemoglobin at High Carbon Monoxide Pressures', in *Probes of Structures and Function of Macromolecules and Membranes, Vol. 2, Probes of Enzymes and Hemoproteins* (1971), Academic Press, New York, 335-342.

163. Reiff, W. M., Long, G. J. and Baken, W. A. Jr., 1968, *Journal of the American Chemical Society* **90**, No. 23, 6347-6351.

164. Reiff, W. M., *Coordintion Chemistry Reviews* Vol. 10 (1973), Elsevier Publishing Co., Amsterdam, 37-77.

165. Rice, F. O. and Teller, E., *The Structure of Matter* (1959), John Wiley and Sons, Inc., New York.

166. Rich, A. and Davison, N., Eds. *Structural Chemistry and Molecular Biology* (1968), W. H. Freeman and Company, San Francisco.

167. Riggs, A. and Imamura, T., 1972, *Advances in Experimental Medicine and Biology* **28**, 55-63.

168. Riggs, A., 1971, *Proc. National Academy of Science U.S.A.* **68**, No. 9, 2062-2065.

169. Riggs, A. and Rona, M., 1969, *Biochimica et Biophysica Acta* **175**, 248-259.

170. Rowe, A. W., Davis, J. H. and Moor-Jankowski, J., *Primates in Medicine* Vol. 7 (1972), Karger, Basel, 117-130.

171. Sadasivan, N., Eberspaecher, H. I., Fuchsman, W. H., and Caughey, W. S., 1969, *Biochemistry* **8**, No. 2, 534-541.

172. Schlemper, E. O. and Hamilton, W. C., 1966, *Inorganic Chemistry* **5**, 995.

173. Sirs, J. A., 'The Interaction of Carbon Dioxide with the Rate of Exchange of Oxygen by Red Blood Cells', in *Blood Oxygenation* (1970), Plenum Press, New York, 116-136.

174. Stöckler, H. A. and Sano, H., 1967, *Physics Letters* **25**(A), 550-551.

175. Strekas, T. C., Packer, A. J. and Spiro, T. G., 1973, *Journal of Raman Spectroscopy* **1**, 197-206.

176. Sugita, Y. and Chanutin, A., 1963, *Proc. Society Exp. Biol. Med.* **112**, 72.

177. Sweeney, W. V., Coucouvanis, D. and Coffman, R. E., 1973, *Journal of Chemical Physics* **59**, No. 1, 369-379.

178. Syrkin, Y. K. and Dyatkina, M. E., *Structure of Molecules and the Chemical Bond* (1969), Interscience Publishers Inc., New York.

179. Tamura, M., Asakura, T. and Yonetani, T., 1973, *Biochimica et Biophysica Acta* **295**, 467-479.

180. Tomita, S. and Riggs, A., 1971, *Journal of Biological Chemistry* **246**, No. 3, 547-554.

181. Tomita, S. and Riggs, A., 1970, *Journal of Biological Chemistry* **245**, No. 12, 3104-3109.

182. Torrens, M. A., Straub, D. K. and Epstein, L. M., 1972, *Journal of the American Chemical Society* **94**, No. 12, 4162-4167.

183. Torrens, M. A., Straub, D. K. and Epstein, L. M., 1972, *Journal of the American Chemical Society* **94**, No. 12, 4160-4162.

184. Trautwein, A. and Harris, F. E., 1975, 'Molecular Orbital Structure, Mossbauer Isomer Shift, and Quadrapole Splitting in Iron Complexes', unpublished.

185. Tsang, C. P., Boyle, A. J. F., and Morgan, E. H., 1973, *Biochimica et Biophysica Acta* **328**, 84-94.

186. Van Hove, L., Hugenholtz, N. M. and Howland, L. P. *Problems in the Quantum Theory of Many Particle Systems* (1961), W. A. Benjamin Inc., New York.

187. Van Vleck, J. H., 1939, *Journal of Chemical Physics* 7, 72.

188. Walch, P. F. and Ellis, D. E., 1973, *Physical Review B* 7, No. 3, 903-907.

189. Watson, J. D., *Molecular Biology of the Gene* (1965), W. A. Benjamin, Inc., New York.

190. Wayland, B. B., Minkiewicz, J. V. and Abd-Elmageed, M. E., 1974, *Journal of the American Chemical Society* **96**, No. 9, 2795-2801.

191. Wertheim, G. K., *Mossbauer Effect: Principles and Applications* (1964), Academic Press, New York.

192. Wicholas, M., Mustacich, R. and Jayne, D., 1972, *Journal of the American Chemical Society* **94**, No. 13, 4518-4521.

193. Wickman, H. H., 'Mossbauer Paramagnetic Hyperfine Structure' in *Mossbauer Effect Methodology* Vol. 2 (1966), Plenum Press, New York, 39-66.

194. Winter, M. R. C., Johnson, C. E., Lang, G. and Williams, R. J. P., 1972, *Biochimica et Biophysica Acta* **263**, 515-534.

195. Zito, R., Antonini, E. and Wyman, J., 1964, *Journal of Biological Chemistry* **239**, No. 6.